https://doi.org/10.5194/egusphere-2026-255
Preprint. Discussion started: 22 January 2026

The efficiency and ocean acidification mitigation potential of ocean alkalinity enhancement on multi-centennial timescales

Hendrik Grosselindemann[1,2], Friedrich A. Burger[1,2], and Thomas L. Frölicher[1,2]

[1]University of Bern, Climate and Environmental Physics, Bern, Switzerland
[2]University of Bern, Oeschger Centre for Climate Change Research, Bern, Switzerland

Correspondence: Hendrik Grosselindemann (hgrosselindemann@gmail.com)

Abstract. Carbon dioxide removal (CDR) strategies such as ocean alkalinity enhancement (OAE) are likely required in addition to rapid emissions reductions to limit global warming to well below 2 °C. However, the long-term efficiency of OAE and its potential to mitigate climate change and ocean acidification remain uncertain. Here, we investigate efficiencies, climate and ocean acidification responses of idealized OAE using a fully coupled, emission-driven Earth system model across three global warming stabilization scenarios (1.5 °C, 2 °C, and 3 °C) spanning 1861-2500. OAE is implemented as a continuous global surface alkalinity addition of 0.14 Pmol yr^{-1} following the CDRMIP protocol from 2026 onward. Our results show that OAE reduces atmospheric CO_2 by 73-130 ppm by 2500, with larger reductions under higher warming scenarios and during the first 100 to 200 years of alkalinity addition. In contrast, global surface air temperature decreases nearly linearly by 0.14-0.17 °C per century across all scenarios, indicating that the cooling rate due to OAE is largely insensitive to the emission pathway and background warming level. The interpretation of OAE efficiency depends strongly on the chosen metric. The global gross ocean carbon capture efficiency of 0.79 remains close to the theoretical maximum, reflecting the negative emissions through OAE, whereas the net ocean capture and atmospheric CO_2 reduction efficiencies are substantially lower and decline over time due to carbon cycle feedbacks in response to lowered atmospheric CO_2. OAE mitigates ocean acidification, at the surface as well as in the interior ocean, with most centennial-scale mitigation arising from atmospheric CO_2 drawdown, an effect shared with other CDR approaches. Direct chemical effects of added alkalinity contribute transiently and diminish over time as the ocean–atmosphere system equilibrates. Overall, our results underscore that rapid emission reductions remain the most effective strategy for achieving the Paris Agreement goals and mitigating ocean acidification.

1 Introduction

Anthropogenic carbon dioxide (CO_2) emissions from fossil fuel combustion and land use change have increased atmospheric CO_2 concentrations by more than 50%, reaching 422 ppm in 2024 (Friedlingstein et al., 2025), higher than at any point in at least the past two million years (IPCC, 2021). This unprecedented increase in greenhouse gas concentrations is the main driver of global surface warming, which averaged about 1.24 °C above pre-industrial levels during 2015-2024 (Forster et al., 2025), and is contributing to more frequent and severe climate extremes both on land and in the ocean (Frölicher et al., 2018; IPCC, 2021). These changes already harm ecosystems and human systems around the world (IPCC, 2022a). Despite ongoing

https://doi.org/10.5194/egusphere-2026-255
Preprint. Discussion started: 22 January 2026

mitigation efforts, emissions reductions remain inadequate, and global temperatures are now on track to exceed the 1.5 °C threshold of the Paris Agreement in the next decade.

Limiting global warming to 1.5 °C will require not only deep decarbonization (IPCC, 2022b; Silvy et al., 2024), but also large-scale carbon dioxide removal (CDR), particularly to offset residual emissions from hard-to-abate sectors such as aviation, cement industry and agriculture (IPCC, 2022b; Bossy et al., 2025). As a result, CDR has become an integral component of national pathways to net-zero emissions (Boehm et al., 2023). While current efforts have largely focused on land-based CDR methods, ocean-based approaches remain comparatively understudied. Among these, ocean alkalinity enhancement (OAE) stands out as one of the most promising due its large carbon sequestration potential, long storage timescales, and potential co-benefits of mitigating ocean acidification (Renforth and Henderson, 2017; IPCC, 2021; National Academies of Sciences, Engineering, and Medicine, 2022; Doney et al., 2025). OAE involves adding alkaline materials, such as olivine or quicklime, to seawater to enhance its natural ability to absorb atmospheric CO_2. Through this process, aqueous CO_2 is converted into bicarbonate and carbonate ions, which are stable forms of inorganic carbon with residence times of 10,000 to 100,000 years (Renforth and Henderson, 2017; Middelburg et al., 2020; National Academies of Sciences, Engineering, and Medicine, 2022; Ho et al., 2023). The resulting depletion of CO_2 in surface waters drives additional oceanic CO_2 uptake, thereby lowering atmospheric CO_2. In addition, by increasing ocean pH, OAE may help counteract ocean acidification and alleviate stress on marine ecosystems (Doney et al., 2009; Bednaršek et al., 2025).

The feasibility of a CDR approach depends on multiple factors, with efficiency and durability of atmospheric CO_2 reduction being particularly critical. Approaches that fail to achieve substantial and long-lasting removal of atmospheric CO_2 are unlikely to be viable. Efficiency, defined as the amount of CO_2 sequestered per unit of alkalinity added, is a key metric for carbon accounting because it determines how much carbon removal can be attributed to an intervention (Boyd et al., 2025). For OAE, efficiency is shaped by three main factors: the ocean's carbonate chemistry, physical ocean processes and global carbon cycle feedbacks. First, the ocean's carbonate chemistry ultimately limits how much additional atmospheric CO_2 can be taken up and stored as dissolved inorganic carbon in response to added alkalinity, thereby setting the theoretical upper limit of efficiency (Renforth and Henderson, 2017). Second, physical ocean processes such as local mixing and air-sea equilibration dynamics exert a strong control on efficiency (He and Tyka, 2023). For example, if added alkalinity is mixed below the surface before equilibration, efficiency initially decreases (Nagwekar et al., 2024; Zhou et al., 2024). The subducted alkalinity may later re-emerge at the surface, often far from deployment site, leading to delayed carbon uptake (Burger et al., 2025). Third, the reduction in atmospheric CO_2 caused by OAE will also decrease oceanic and terrestrial CO_2 uptake, which in turn feeds back on atmospheric CO_2 and reduces overall efficiency (Schwinger et al., 2024; Jeltsch-Thömmes et al., 2024). Similarly, ocean-internal biogeochemical feedbacks, mostly through calcifying organisms, can influence efficiency (Lehmann and Bach, 2025).

To date, most modelling studies on OAE efficiency have used simplified Earth system models or forced ocean-only configurations (Tyka et al., 2022; He and Tyka, 2023; Nagwekar et al., 2024; Jeltsch-Thömmes et al., 2024; Zhou et al., 2024; Martin et al., 2025). Many of these studies prescribe atmospheric CO_2, thereby neglecting changes in oceanic and terrestrial carbon uptake that would result from OAE-induced reductions in atmospheric CO_2, or they focus only on relatively short timescales

https://doi.org/10.5194/egusphere-2026-255
Preprint. Discussion started: 22 January 2026

(decadal to multi-decadal). However, simulations with fully coupled, emission-driven Earth system models are essential to capture the full carbon cycle response, especially over multi-centennial time scales, and its dependence on background climate state and emissions pathways (Fennel et al., 2023; Palmiéri and Yool, 2024; Schwinger et al., 2024; Lehmann and Bach, 2025; Tyka, 2025). Only a few of such fully coupled modelling studies exist, and they consistently show that interactions among the atmosphere, ocean, and land biosphere strongly reduce OAE efficiency compared to modelling experiments with prescribed atmospheric CO_2 (Jeltsch-Thömmes et al., 2024; Schwinger et al., 2024; Tyka, 2025; Wey et al., 2025; Sathyanadh et al., 2025; Nagwekar et al., 2026).

Another key knowledge gap concerns the potential of OAE to mitigate ocean acidification, often discussed as a valuable co-benefit of OAE (Bach et al., 2019). Global OAE simulations with single Earth system models indicate a reduction in global and regional ocean acidification (Ilyina et al., 2013; Feng et al., 2016; Mongin et al., 2021; Jin and Cao, 2025), and local real-world experiments show that OAE can enhance pH and support calcification in vulnerable ecosystems such as coral reefs (Albright et al., 2016). However, the magnitude and persistence of OAE-induced pH changes, both globally and regionally, remain uncertain, as previous studies rely on theoretical concepts (van de Mortel et al., 2025) or simplified, coarse-resolution models (Ilyina et al., 2013; Jin and Cao, 2025; Findlay et al., 2025). As with OAE efficiency, addressing these uncertainties requires comprehensive Earth system models capable of capturing global carbon cycle feedbacks (Butenschön et al., 2021; Bednaršek et al., 2025).

In this study, we investigate multiple OAE efficiency metrics and assess the OAE-induced carbon cycle, climate and ocean acidification responses under multi-centennial global warming stabilization scenarios using a comprehensive fully coupled Earth system model. We first describe the model setup and simulation scenarios, followed by the definition of efficiency metrics and the processes governing pH changes. We then assess the climate and carbon cycle response, the temporal and spatial evolution of OAE efficiencies, and the ocean acidification mitigation potential. Finally, we discuss our findings and place it in the context of existing literature.

2 Methods

2.1 GFDL ESM2M model

This study uses the fully-coupled GFDL-ESM2M Earth system model developed at the NOAA Geophysical Fluid Dynamics Laboratory (Dunne et al., 2012, 2013). The individual components of the model are the modular ocean model version MOM4p1 (Griffies et al., 2009), the atmospheric model version AM2 (Anderson, Jeffrey L. et al., 2004), the land model version LM3 (Shevliakova et al., 2009) and the sea-ice model from Winton (2000). The atmosphere and land components have a nominal horizontal resolution of 2x2.5°. The ocean model has a horizontal resolution of 1°, which increases to 0.3° near the equator. It has 50 vertical levels, with a layer thickness of 10 m in the upper 200 m gradually increasing to 300m at greater depths. Additionally, the ocean model is coupled to the biogeochemistry model TOPAZv2, which simulates 30 biogeochemical tracers to represent cycling of carbon and alkalinity, as well as active pelagic calcite and aragonite and their sediment interaction (Dunne et al., 2013). Three phytoplankton groups and implicit zooplankton grazing actively influence the production and

https://doi.org/10.5194/egusphere-2026-255
Preprint. Discussion started: 22 January 2026

remineralisation of carbon and alkalinity. Pelagic calcite and aragonite production depends on the respective saturation state and this detritus sinks through the water column and can be dissolved or deposited in the sediments, from where it can either be stored or redissolved. Ocean carbonate chemistry follows routines from the OCMIP2 protocol (Najjar and Orr, 1998). The land model simulates the cycling of carbon, including different vegetation types, soils, wildfires and harvesting.

The model has been shown to perform well in representing the global carbon cycle (Dunne et al., 2013; Bopp et al., 2013; Frölicher et al., 2015; Séférian et al., 2020; Burger et al., 2022). It simulates anthropogenic carbon uptake and storage close to observations (Frölicher et al., 2015; Bronselaer et al., 2017), and it represents alkalinity well by actively simulating both calcite and aragonite cycling in comparison to other climate models (Planchat et al., 2023).

2.2 Simulations setup

A set of different model simulations with and without ocean alkalinity enhancement were performed for this study (Fig. 1). After an initial spin-up (Burger et al., 2020), an emission-driven historical simulation was performed over the period 1861 to 2005, which follows observed fossil fuel and land-use change CO_2 emissions and prescribed non-CO_2 radiative forcing agents. This simulation was continued for 20 simulation years in which fossil fuel CO_2 emissions followed observed emissions until 2020 and national determined contributions until 2025 (Silvy et al., 2024). From 2026 on, the adaptive emission reduction approach (AERA) was applied to reach a specified global warming level. This algorithm adapts the allowable future fossil fuel CO_2 emissions every five years based on the current warming level and the remaining CO_2 forcing equivalent (CO_2-fe) emission budget estimated by the transient climate response to cumulative CO_2-fe emissions (TCRE-fe) (Terhaar et al., 2022). Three target warming levels of 1.5, 2.0 and 3.0 °C above pre-industrial were chosen to cover a range of possible global warming scenarios. These simulations were run until 2500 to investigate changes on multi-centennial timescales under temperature stabilization (labelled as 'Ref' in Figures). Non-CO_2 radiative forcing agents and land-use change were following the RCP2.6 scenario after 2005 in all future warming simulations and are kept constant after 2100 (Silvy et al., 2024).

The Ocean Alkalinity Enhancement (OAE) experiments follow the same CO_2 emission and non-CO_2 forcing pathways as the reference simulations (labelled as 'OAE' in Figures). OAE is implemented following the protocol defined by the Carbon Dioxide Removal Model Intercomparison Project (CDRMIP) (Keller et al., 2018b). A total of $0.14\,\mathrm{Pmol\,yr^{-1}}$ of alkalinity is continuously and homogeneously added to the global surface ocean, excluding regions south of 60°S and north of 70°N, as they are seasonally sea-ice covered and therefore a year-round input of alkalinity to the surface ocean may not be possible. Although this magnitude and spatial distribution of alkalinity input is unlikely to be achievable with current or near-future societal means (Eisaman et al., 2023), it provides a useful framework for exploring impacts of global-scale OAE and facilitates comparison with other model-based studies using the same framework (Keller et al., 2018b; Köhler, 2020; Qu et al., 2025; Wey et al., 2025).

Following the approach of Schwinger et al. (2024), we perform a third set of simulations to assess feedback processes that influence the efficiency of OAE (labelled as 'Ref*' in Figures). These simulations are driven by prescribed atmospheric CO_2 concentrations from the 'OAE' run (which is lower than in the REF run) and therefore simulate the same climate trajectory as the 'OAE' simulations, but without the addition of the alkalinity. The simulations thus exclude any additional atmospheric

https://doi.org/10.5194/egusphere-2026-255
Preprint. Discussion started: 22 January 2026

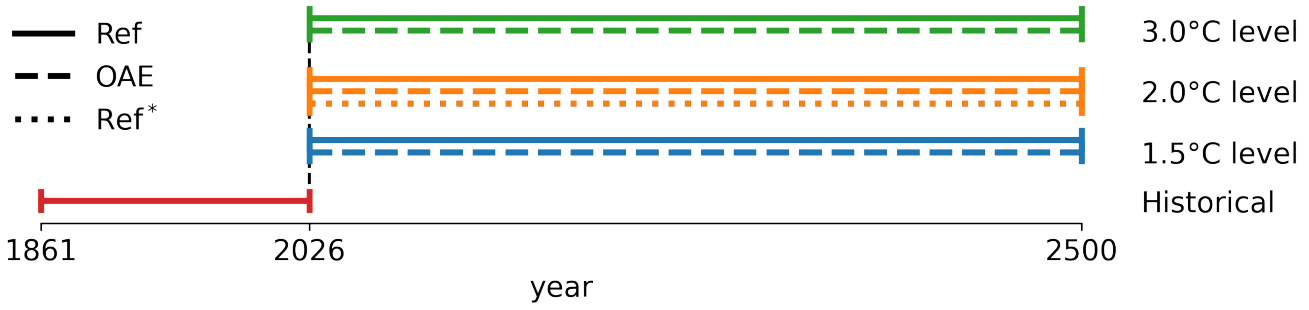

Figure 1. Schematic overview of all simulations conducted in this study. All simulations are branched in 2026 from simulations that follow historical fossil fuel and land-use change CO_2 emissions along with other non-CO_2 radiative forcing agents. The reference simulations (Ref) stabilize global surface air temperature at 1.5 °C, 2 °C and 3 °C without ocean alkalinity enhancement (OAE). Corresponding OAE simulations follow the same emission pathways but include alkalinity enhancement. An additional 2 °C reference simulation (Ref*) follows prescribed atmospheric CO_2 from the OAE 2 °C simulation, but without OAE. Each configuration is run with five ensemble members each.

CO_2 removal by the ocean due to OAE. These additional simulations help to isolate the OAE effect by removing global carbon feedback processes. We conducted those simulations only for the 2 °C warming level, as it is sufficient to illustrate the relevant processes, which can be generalized to other warming levels.

For all scenarios, we have conducted a five-member perturbed initial-condition ensemble. An initial-condition ensemble enables the separation of the forced climate response from uncertainties arising from natural internal variability (Frölicher et al., 2009; Deser et al., 2020). We set up the ensembles with a sea surface temperature perturbation on the order of 10^{-5} °C at one grid point in the Weddell Sea on January 1st, 1861 (Burger et al., 2020; Frölicher et al., 2020).

2.3 Definitions of OAE efficiencies

Several complementary metrics can be used to assess OAE efficiency, each capturing different aspects. These metrics are explained in the following and illustrated, along with the associated carbon fluxes, in Fig. 2.

2.3.1 Maximum ocean capture efficiency

The maximum ocean capture efficiency $\eta_{o,max}$ of OAE is derived purely from the carbonate chemistry of seawater. It represents the change in dissolved inorganic carbon (DIC) resulting from the addition of alkalinity (ALK), assuming the oceanic pCO_2 fully re-equilibrates to the pCO_2 before alkalinity addition and is calculated at the ocean surface (Frankignoulle et al., 1994; Renforth and Henderson, 2017; Tyka et al., 2022). It can be expressed as the ratio of the sensitivity of the seawater partial pressure of CO_2 (pCO_2) to changes in alkalinity versus its sensitivity to changes in dissolved inorganic carbon (DIC):

$$\eta_{o,max} = -\frac{\partial pCO_2}{\partial ALK} \Big/ \frac{\partial pCO_2}{\partial DIC} \tag{1}$$

https://doi.org/10.5194/egusphere-2026-255
Preprint. Discussion started: 22 January 2026

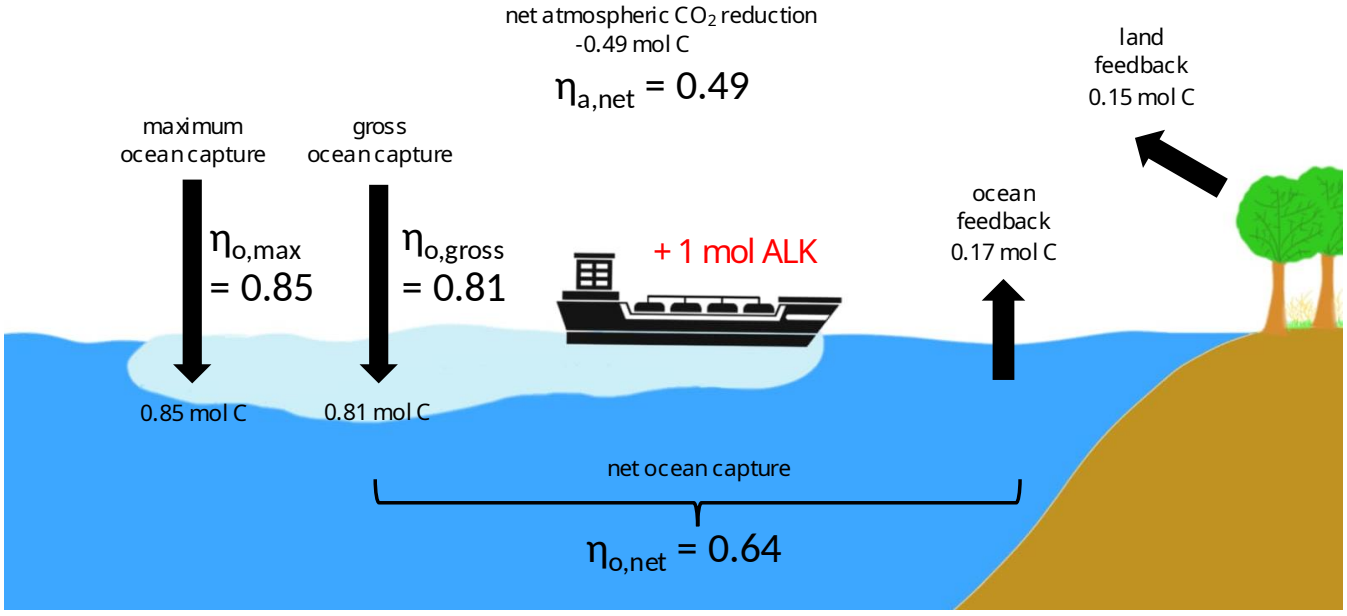

Figure 2. Schematic illustration of OAE efficiency metrics and associated carbon transfer of adding, for example, 1 mol of alkalinity to the surface ocean. The carbon transfer per added alkalinity are the ensemble average of the first 100 years in the 2 °C simulation. The metrics include maximum ocean capture efficiency $\eta_{o,max}$, net ocean capture efficiency $\eta_{o,net}$, gross ocean capture efficiency $\eta_{o,gross}$ and net atmospheric CO_2-reduction $\eta_{a,net}$

We use MOCSY to calculate sensitivities of the oceans' pCO_2 to dissolved inorganic carbon and alkalinity with units of $\frac{\mu atm}{mol/kg}$ (Orr and Epitalon, 2015). A $\eta_{o,max}$ value of 0.8 indicates that an addition of 1 mol kg^{-1} of alkalinity can potentially increase ocean carbon content by 0.8 mol kg^{-1}.

2.3.2 Net ocean capture efficiency

In reality, not all of the potential ocean carbon uptake is realised. We therefore quantify the net ocean capture efficiency $\eta_{o,net}$, which accounts for both the ocean's feedback to the OAE-induced reduction of atmospheric CO_2 and the horizontal and vertical redistribution of added alkalinity by physical ocean processes before full equilibration with the atmosphere (Schwinger et al., 2024). The atmospheric CO_2 is also influenced by the land carbon feedback (i.e. reduced terrestrial CO_2 uptake due to lower atmospheric CO_2), buffering part of the OAE-induced reduction in atmospheric CO_2 (Keller et al., 2014, 2018a). The net ocean capture efficiency $\eta_{o,net}$ is defined as the ratio of the change in air-sea CO_2 flux to the amount of alkalinity added:

$$\eta_{o,net} = \frac{F_{CO_2}^{OAE} - F_{CO_2}^{Ref}}{F_{ALK}} \tag{2}$$

https://doi.org/10.5194/egusphere-2026-255
Preprint. Discussion started: 22 January 2026

Here, F_{CO_2} refers to the air-sea CO_2 flux in $\mathrm{Pmol\,yr^{-1}}$. The nominator represents the additional CO_2 uptake by the ocean in the 'OAE' simulation relative to the reference simulation 'Ref', both following the same emissions trajectory. F_{ALK} denotes the rate of alkalinity addition of $0.14\,\mathrm{Pmol\,yr^{-1}}$.

2.3.3 Gross ocean capture efficiency

To quantify the carbon flux resulting solely from alkalinity addition and the redistribution of added alkalinity by physical ocean processes before equilibration with the atmosphere, excluding the ocean and land carbon feedbacks in response to the OAE-induced reduction of atmospheric CO_2, we define the gross ocean capture efficiency, $\eta_{o,gross}$ (Schwinger et al., 2024; Zhou et al., 2024; Tyka, 2025):

$$\eta_{o,gross} = \frac{F_{CO_2}^{OAE} - F_{CO_2}^{Ref^*}}{F_{ALK}}. \tag{3}$$

It is calculated by subtracting the air-sea CO_2 flux of the Ref* simulation from that of the OAE simulation, and dividing the result by the amount of alkalinity added in the OAE simulation. The Ref* simulation shares the same climate state as the OAE simulation, but oceanic CO_2 uptake is not driven by OAE. The difference between the OAE and Ref* simulations eliminates the natural carbon fluxes and feedback processes between reservoirs, thereby leaving the total additional ocean carbon uptake due to OAE. We did an extra experiment to prove that this additional ocean carbon uptake leads to the same reduction in atmospheric CO_2 as direct air capture (Appendix A) and it therefore represents negative emissions.

2.3.4 Net atmospheric CO_2 reduction efficiency

The fourth efficiency metric used in this study is the net atmospheric CO_2 reduction efficiency $\eta_{a,net}$:

$$\eta_{a,net} = \frac{R_{CO_2}^{OAE} - R_{CO_2}^{Ref}}{F_{ALK}}. \tag{4}$$

It describes the difference between the change in atmospheric CO_2 inventory per year (R_{CO_2} in $\mathrm{Pmol\,yr^{-1}}$) between the OAE simulation and the Ref simulation divided by the yearly addition of alkalinity (Jeltsch-Thömmes et al., 2024; Tyka, 2025). This metric describes the potential of OAE to reduce atmospheric CO_2 and therefore global warming.

2.4 Drivers of ocean acidification mitigation

Three processes drive the total pH response to OAE: reduction in atmospheric CO_2, pH hysteresis, and pCO_2 disequilibrium:

$$\Delta pH_{total} \simeq \Delta pH_{CDR} + \Delta pH_{hysteresis} + \Delta pH_{disequilibrium} \tag{5}$$

The three processes are described in the following.

2.4.1 Reduction in atmospheric CO_2

Any CDR method that lowers atmospheric CO_2, being terrestrial or marine, mitigates ocean acidification, as seawater loses carbon when equilibrating to the lowered atmospheric pCO_2. This CDR-driven pH increase can be quantified using the Ref*-

https://doi.org/10.5194/egusphere-2026-255
Preprint. Discussion started: 22 January 2026

simulation, which follows the atmospheric CO_2 trajectory of the OAE simulation, but excludes alkalinity addition. The resulting pH difference relative to the Ref-simulation represents the pH change due to CDR:

$$\Delta pH_{CDR} = pH^{Ref^*} - pH^{Ref} \tag{6}$$

2.4.2 pH hysteresis

The pH hysteresis effect arises because the sensitivities of pCO_2 and pH to changes in dissolved inorganic carbon (DIC) and total alkalinity differ. When oceanic pCO_2 is lowered through alkalinity addition and subsequently returns to the original value through air-sea carbon uptake, both alkalinity and DIC are higher than before alkalinity addition. As a result, pH is higher than before the intervention. We refer to this as the "pH hysteresis" effect, where identical pCO_2 levels correspond to different carbonate system and pH states before and after alkalinity addition. The contribution of this effect to the total pH change can be estimated from the ocean carbonate system and the alkalinity perturbation relative to the reference state (full derivation in Appendix B).

$$\Delta pH_{hysteresis} \simeq \eta_{o,max} \frac{\Delta ALK}{ALK^{Ref}} \frac{1}{ln(10)} \tag{7}$$

2.4.3 pCO_2 disequilibrium

During oceanic pCO_2 equilibration with the atmosphere after alkalinity addition, the temporarily lower pCO_2 in seawater leads to an increase in pH. We can quantify this contribution by manipulating the ocean carbonate system offline. We use the oceanic conditions from the OAE simulation (i.e. alkalinity, pCO_2, temperature, salinity, phosphate and silicate concentrations), where pCO_2 in the ocean remains depressed because re-equilibration with the atmosphere is incomplete. The offset in oceanic pCO_2 is calculated as the difference between the OAE and Ref*-simulation: $\Delta pCO_2 = pCO_2^{Ref^*} - pCO_2^{OAE}$, which isolates the effect of alkalinity addition since both simulations share the same atmospheric CO_2. We then recompute the carbonate system for OAE conditions but add ΔpCO_2 to restore full air-sea equilibrium using the pyCO2SYS package (Humphreys et al., 2022). This yields the carbonate system state after equilibration (i.e., when $\Delta pCO2 = 0$). The pH change associated with the pCO_2 disequilibrium is then given by:

$$\Delta pH_{Disequilibrium} = pH^{OAE} - pH^{OAE+\Delta pCO_2} \tag{8}$$

3 Results

3.1 Atmospheric CO_2 and global temperature response

In the Ref simulations without OAE, global surface air temperature stabilizes at the prescribed global warming levels (solid lines in Fig. 3a). Specifically, the 1.5 °C stabilization is reached in year 2068 [5-member ensemble range: 2043-2113], the 2 °C stabilization in year 2109 [2101-2124] and the 3 °C stabilization in year 2183 [2177-2197], calculated following Lacroix et al. (2024). In each case, CO_2 emissions decline to zero and subsequently become slightly negative (Fig. C1), which is

https://doi.org/10.5194/egusphere-2026-255
Preprint. Discussion started: 22 January 2026

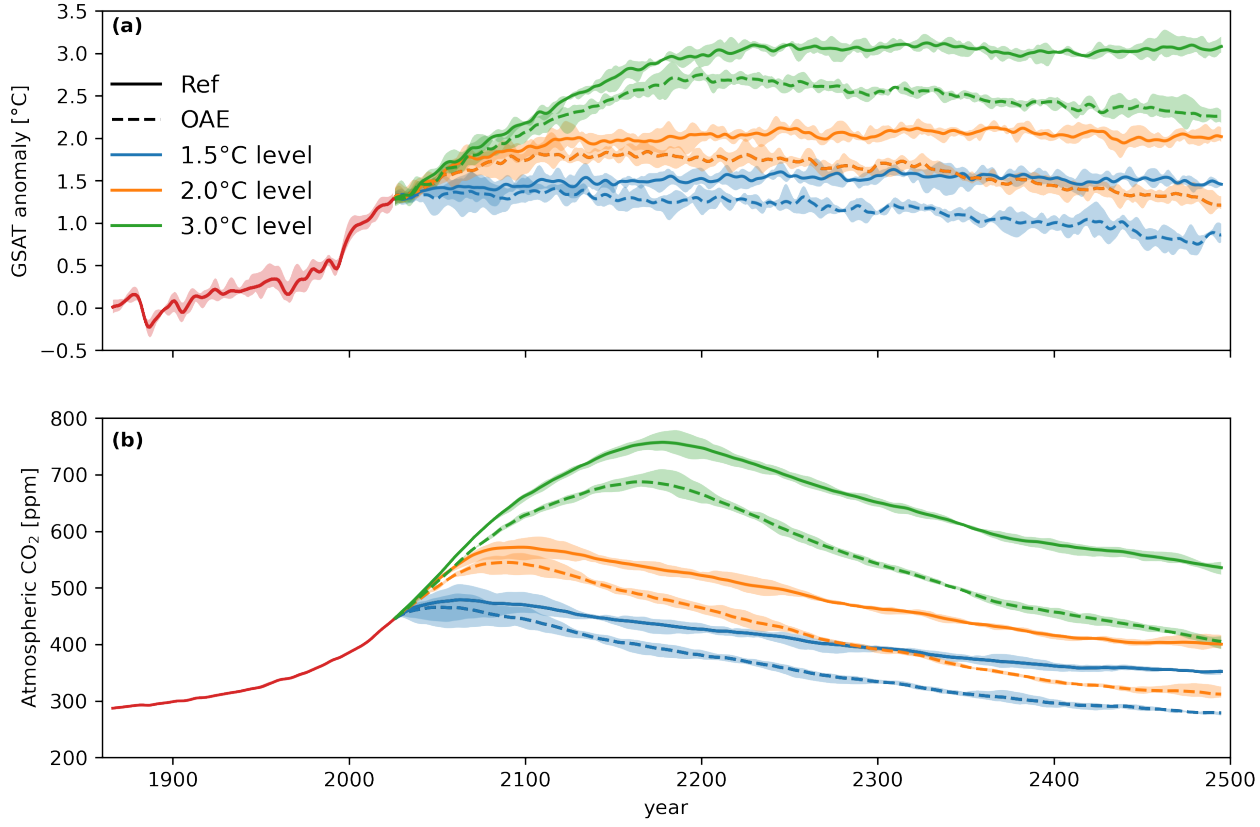

Figure 3. Global surface air temperature (a) and atmospheric CO_2 (b) over 1861 to 2500 under three different global warming stabilization scenarios with and without OAE. Red lines show the 1861-2025 historical period. Solid lines are the reference simulation (Ref) and dashed lines are simulations with ocean alkalinity enhancement (OAE). All lines are ensemble and 31-year running means, while the shading represents the ensemble range.

required to maintain the stabilized warming levels through the year 2500, as the GFDL-ESM2M model has a positive zero emission commitment on multi-centennial timescale (Frölicher et al., 2014; Frölicher and Paynter, 2015; Silvy et al., 2024). The 31-year mean atmospheric CO_2 concentration peaks at 484 ppm [455-504] in 2074 [2052-2102] in the 1.5 °C scenario, at 573 ppm [551-589] in 2096 [2081-2112] in the 2 °C scenario and at 758 ppm [742-777] in 2176 [2164-2186] in the 3 °C scenario (Fig. 3b). Thereafter, atmospheric CO_2 decreases due to the continuous uptake of carbon by the terrestrial biosphere and predominately by the ocean.

In the OAE simulations, the continuous addition of alkalinity to the surface ocean causes additional carbon uptake from the atmosphere and reduces atmospheric CO_2 concentrations compared to the reference simulations without OAE (dashed lines in Fig. 3b). The 31-year mean peak atmospheric CO_2 is lower and earlier than without OAE: at 468 ppm [437-488] in year 2059 [2041-2088] in the 1.5 °C scenario, at 546 ppm [524-560] in year 2085 [2076-2097] in the 2 °C scenario and at 689 ppm

https://doi.org/10.5194/egusphere-2026-255
Preprint. Discussion started: 22 January 2026

[677-708] in year 2167 [2158-2178] in the 3 °C scenario. The decrease in atmospheric CO_2 increases with the amount of global warming. Atmospheric CO_2 concentrations are 73 ppm [72-74] lower in the 1.5 °C scenario, 88 ppm [86–88] lower in the 2 °C scenario, and 130 ppm [130-131] lower in the 3 °C scenario relative to their respective reference simulations between 2470 and 2500 (Fig. 4a-c). The greatest reductions occur within the first 100 (1.5 °C scenario) to 200 (3 °C scenario) years following the start of alkalinity addition (Fig. 4a-c), after which the differences increases less towards the end of the simulations (explained in Sec. 3.3).

The reduction in atmospheric CO_2 under OAE reduces global surface air temperature relative to the reference scenarios (Fig. 3a). Global surface air temperature is 0.64 °C [0.57-0.71] lower in the 1.5 °C scenario, 0.75 °C [0.68–0.80] lower in the 2 °C scenario, and 0.79 °C [0.65-0.96] lower in the 3 °C scenario compared to their respective references between 2470 and 2500. Unlike atmospheric CO_2 concentrations, which showed the largest differences developing shortly after alkalinity addition, the surface temperature difference increases approximately linearly throughout the simulation in all scenarios (Fig. 4d-f). In the 2 °C scenario, the global surface air temperature decreases linearly by -0.16 °C per century [-0.15 to -0.17]. This near-linear trend reflects the logarithmic relationship between radiative forcing and CO_2. Using the formulation of Myhre et al. (1998), $\Delta F = -5.35 Wm^{-2} ln(CO_2^{Ref}/CO_2^{OAE})$, we estimate a near-linear reduction in radiative forcing of $-0.31\,\mathrm{Wm^{-2}}$ per century [-0.31 to -0.32] (R^2 of 0.97), yielding a total decrease of $-1.35\,\mathrm{Wm^{-2}}$ [-1.42 to -1.30] by 2500. The temperature trend is slightly lower for the 1.5 °C scenario with a cooling of -0.14 °C per century [-0.13 to -0.15], associated with a slightly lower trend in radiative forcing of $-0.30\,\mathrm{Wm^{-2}}$ per century [-0.29 to -0.30] (R^2 of 0.95) in the 1.5 °C scenario. The cooling is largest in the 3 °C scenario with -0.17 °C per century [-0.16 to -0.19] based on a higher reduction in radiative forcing of $-0.34\,\mathrm{Wm^{-2}}$ per century [-0.33 to -0.34] (R^2 of 0.99). The trends in radiative forcing show only small variations between scenarios, even though the reductions in atmospheric CO_2 concentrations due to OAE differ much more. This is due to similar ratios of CO_2 between the reference scenario and the OAE simulations across warming levels, but slightly higher for a warmer climate. Consequently, the three scenarios exhibit comparable cooling trends despite their differing CO_2 trajectories, although the exact temperature response may also be influenced by scenario-dependent climate feedbacks and ocean heat uptake.

The regional temperature response broadly mirrors the global warming pattern, but with opposite sign (Fig. C2a-c). Cooling is strongest over continents and at high northern latitudes, and weaker over the ocean, particularly in the Southern Ocean. An exception to the overall cooling occurs in the northern North Atlantic, where a localized warming develops in the higher warming scenarios. This North Atlantic warming reflects an earlier and stronger recovery of the Atlantic Meridional Overturning Circulation under OAE, which enhances ocean heat transport into the region (not shown). This effect is most pronounced in the 3 °C scenario.

3.2 Global carbon flux response

Ocean alkalinity enhancement leads to substantial additional ocean carbon uptake and lowers atmospheric CO_2, but part of this drawdown is offset by carbon release from the land biosphere (Figure 5). In the reference simulations, the total cumulative ocean carbon uptake since pre-industrial increases rapidly initially with increasing CO_2 emissions and slows markedly toward the end of the simulation when global warming is stabilized (solid blue lines in Figure 5). OAE leads to a persistent additional

https://doi.org/10.5194/egusphere-2026-255
Preprint. Discussion started: 22 January 2026

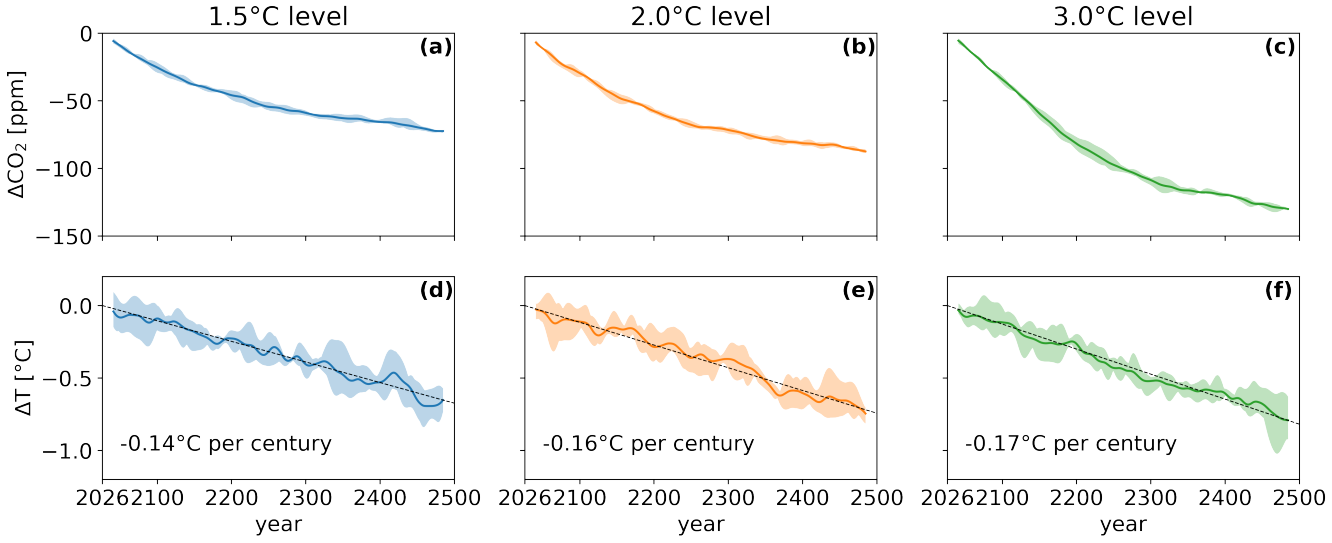

Figure 4. Difference in annual mean atmospheric CO_2 (a-c) and global surface air temperature (d-f) between the ocean alkalinity enhancement (OAE) and reference (Ref) simulations over time for the three global warming stabilization scenarios 1.5 °C (a,d), 2 °C (b,e) and 3 °C (c,f). All lines are ensemble and 31-year running means, while the shading represents the ensemble range. Dashed black lines in (d-f) show the linear trend and its estimates are noted.

increase in cumulative ocean carbon uptake relative to the reference scenario (dashed blue lines in Figure 5). By year 2500, cumulative ocean carbon uptake is higher by 362 PgC [356-366], 380 PgC [377-383] and 407 PgC [403-412] in the 1.5 °C, 2 °C, and 3 °C scenarios, respectively. When feedbacks that redistribute carbon among reservoirs are neglected, the cumulative ocean uptake is substantially larger. In the 2 °C scenario, this gross cumulative ocean carbon uptake attributable to OAE (the difference between OAE and Ref*) amounts to 628 PgC [625-632], approximately 65% larger than the net uptake. This difference arises because reduced atmospheric CO_2 concentrations due to OAE result in an anomalous outgassing of carbon stored in the ocean, thereby offsetting the gross ocean carbon uptake due to OAE. The reduction in atmospheric CO_2 is modulated by anomalous carbon release from the land biosphere. In the 2 °C scenario, this land carbon release totals 194 PgC [189–198], resulting in a net atmospheric carbon reduction of 189 PgC [185–192]. The land carbon response varies across warming levels. The net carbon release from land is largest in the 1.5 °C scenario at 209 PgC [196–218] and smallest in the 3 °C scenario at 129 PgC [122–134]. Consequently and following the ocean carbon uptake, the net atmospheric CO_2 reduction is largest in the 3 °C scenario (279 PgC [271–284]) and smallest in the 1.5 °C scenario (156 PgC [149–164]).

Regionally, OAE leads to enhanced cumulative net carbon uptake in most ocean regions (Fig. 6a), with particularly strong uptake along western boundary currents and north of the Antarctic Circumpolar Current. However, some regions become anomalous cumulative carbon sources over time (i.e., these regions lose carbon to the atmosphere relative to the reference simulation without OAE). Most notably, the Southern Ocean south of 60° S shows net outgassing, as no alkalinity is added in these regions and the lower atmospheric CO_2 leads to anomalous outgassing. A similar signals emerges south of the eastern

https://doi.org/10.5194/egusphere-2026-255
Preprint. Discussion started: 22 January 2026

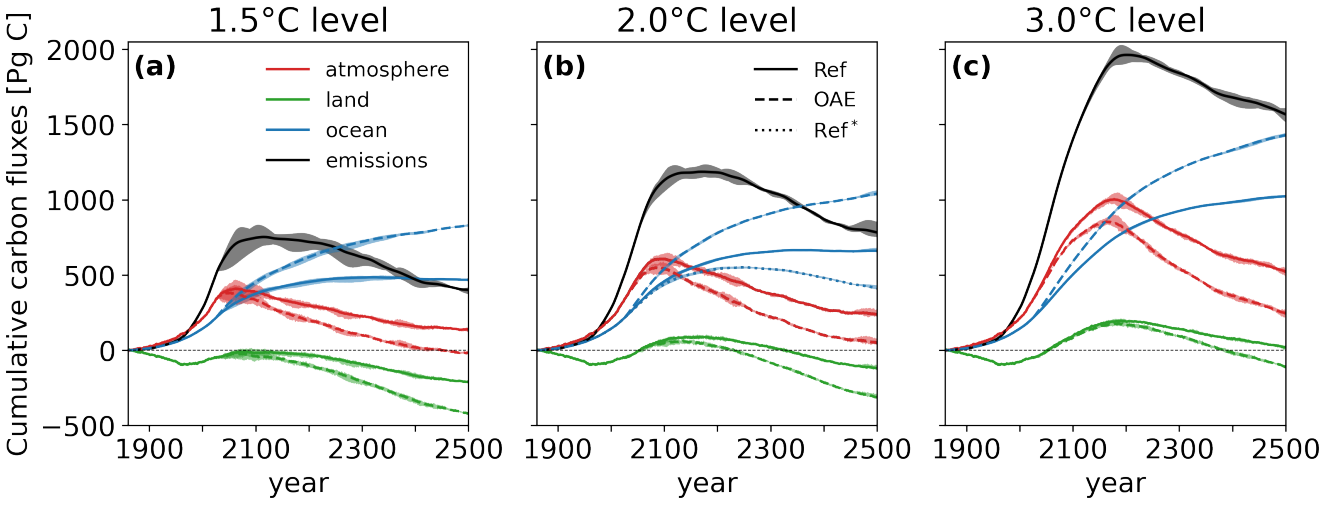

Figure 5. Cumulative globally integrated carbon fluxes since pre-industrial for the atmosphere (red), land (green, including land-use changes), and ocean (blue), as well as fossil fuel CO_2 emissions (black) for the reference simulations (Ref), ocean alkalinity enhancement (OAE) and the additional reference simulation (Ref*) under the 1.5 °C, 2 °C and 3 °C (a-c) global warming scenarios. All lines show ensemble means and shading indicates the ensemble range.

tropical Pacific. There, added alkalinity produces only a weak local reduction in oceans pCO_2 due to high buffer capacity and low accumulation of alkalinity, while atmospheric pCO_2 is reduced more strongly by global OAE, leading to a negative air-sea pCO_2-gradient and hence outgassing in this regions. The land biosphere exhibits widespread carbon loss, with strong spatial variability in magnitude (Fig. 6a). The gross cumulative ocean carbon uptake attributable to OAE (difference between OAE and Ref*) is positive everywhere (Fig. 6b) and closely resembles the spatial pattern of cumulative anthropogenic carbon uptake (Frölicher et al., 2015). Spatial uptake patterns are relatively uniform during the first century but become increasingly heterogeneous over time. As the atmospheric CO_2 levels in the REF* and OAE simulations are identical, the land shows no significant changes in carbon fluxes (Fig. 6b).

3.3 Ocean alkalinity enhancement efficiency

The simulated carbon cycle response and differences between warming levels relate to the efficiency of OAE. The four metrics to assess the global efficiency of OAE (Sec. 2.3) differ strongly in their absolute values, temporal evolution, and sensitivity to the global warming stabilization level and emission pathway (Fig. 7). The maximum ocean capture efficiency at the surface, determined solely by the response of seawater carbonate chemistry to alkalinity addition, remains nearly constant over time and across the three warming levels at 0.81-0.86 (black lines in Fig. 7). However, it increases slightly at higher atmospheric CO_2, where the ocean buffer capacity is reduced (Fig. C3). At lower buffer capacities, the sensitivity of ocean pCO_2 to changes in alkalinity increases relative to that with respect to dissolved inorganic carbon, allowing for an increased uptake of carbon to

https://doi.org/10.5194/egusphere-2026-255
Preprint. Discussion started: 22 January 2026

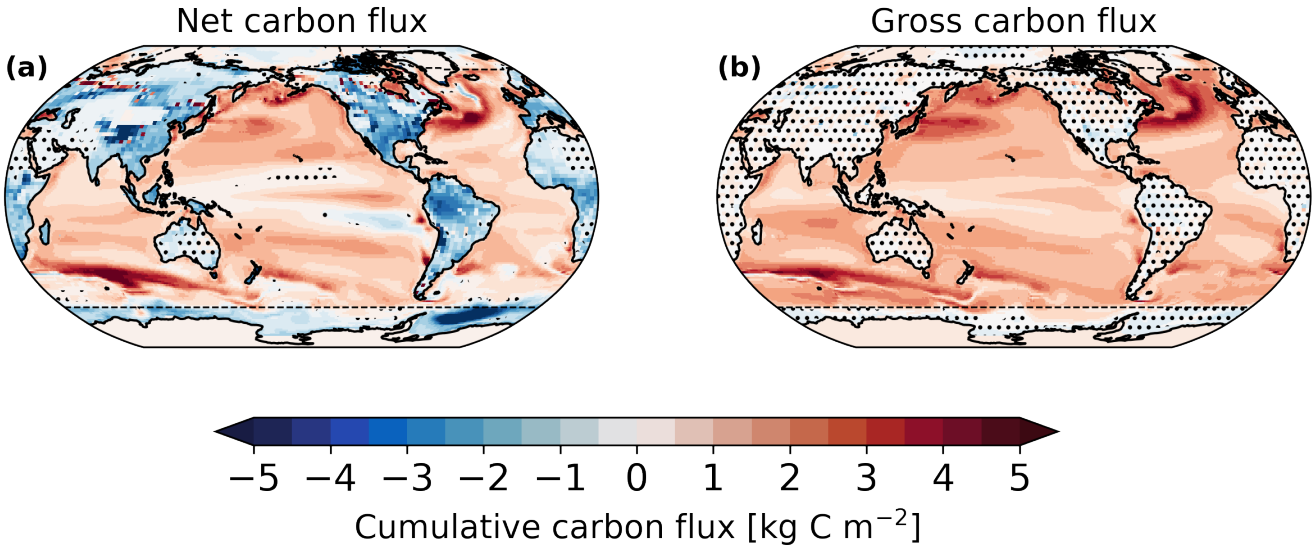

Figure 6. Spatial maps of cumulative net carbon fluxes (difference between OAE and Ref simulation) from 2026 to 2500 for the 2 °C warming scenario in (a) and the gross carbon fluxes (difference between OAE and Ref*) in (b). Colors show ensemble means and hatchings show differences that are not significant at the 95% confidence level based on a two-sided Students t-test. Dashed black lines mark the regions north of 70°N and south of 60°S, where alkalinity addition is not applied.

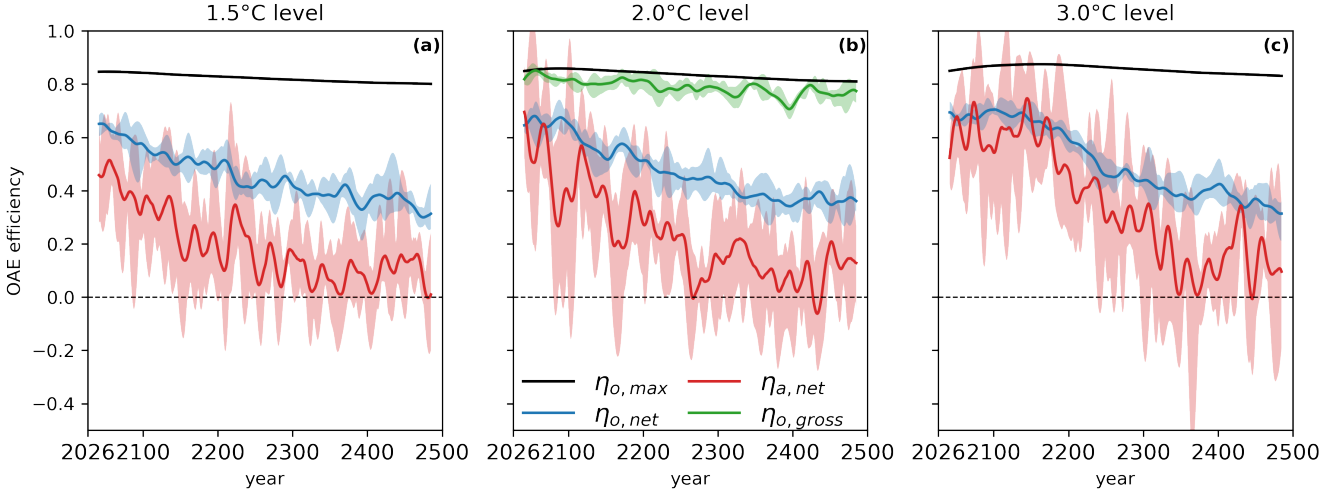

Figure 7. Annual efficiencies of ocean alkalinity enhancement for the three global warming stabilization scenarios 1.5 °C, 2 °C and 3 °C (a-c). Maximum ocean capture efficiency $\eta_{o,max}$ in black, net ocean capture efficiency $\eta_{o,net}$ in blue, net atmospheric CO_2-reduction $\eta_{a,net}$ in red and gross ocean capture efficiency $\eta_{o,gross}$ in green. All lines are ensemble and 31-year running means, while the shading represents the ensemble range.

https://doi.org/10.5194/egusphere-2026-255
Preprint. Discussion started: 22 January 2026

balance an alkalinity-induced reduction of pCO_2. As a result, efficiencies are slightly higher at peak atmospheric CO_2 and in the 3.0°C scenario compared to the 1.5°C case.

The net ocean capture efficiency, defined as the change in net air-sea CO_2 flux per unit of alkalinity added, is consistently lower than the maximum efficiency and declines over time (blue lines in Fig. 7). Before peak atmospheric CO_2, efficiencies range between 0.64-0.68 with little variation between scenarios, but slightly higher in warmer scenarios. After the peak, they drop to 0.35-0.36 by 2400-2500, reflecting a gradual long-term decrease. This temporal decline is a result of five interacting processes that are qualitatively discussed: the redistribution of alkalinity within the ocean interior, changes in the ocean buffer capacity, carbon effluxes from the land biosphere and ocean internal changes of alkalinity and DIC by biological activity. First, the added alkalinity undergoes vertical mixing and thereby, the volume in exchange with the atmosphere, over which the equilibration with the atmosphere occurs, increases steadily over time. The larger the volume, the more old carbon-rich waters are being upwelled to the surface and see an atmosphere with reduced atmospheric CO_2 concentration, resulting in anomalous outgassing to the atmosphere and hence lowering net ocean carbon uptake. We use the effective mixed layer depth from Zhou et al. (2024) as a proxy for the volume of the ocean that is in exchange with the atmosphere. Scenarios show negligible differences in magnitude and temporal change in this volume, with the effective mixed layer depth increasing near-linearly from around 140 m in 2026 to about 1400 m in 2500 (not shown), leading to a steady decrease in efficiency. Second, a low ocean buffer capacity means that the change in oceanic pCO_2 per change in dissolved inorganic carbon is large compared to the sensitivity of atmospheric pCO_2 to the atmospheric carbon content. In this case, a lot of carbon is taken up by the ocean until both systems equilibrate at an intermediate pCO_2 and efficiency is high. The buffer capacity is lower in the high warming scenarios and decreases before peak atmospheric CO_2 and increases afterwards in each scenario (Fig. C3). As the timing of peak CO_2 differs between scenarios, so does the influence of buffer capacity onto the efficiency. Third, the reduction in atmospheric CO_2 by ocean carbon uptake is buffered by a relative efflux of carbon from the land biosphere. This increases atmospheric pCO_2 and allows for more ocean carbon uptake until equilibrium is reached, increasing efficiency. We find a steady increase in the cumulative land efflux over time and largest effluxes in the 1.5 °C scenario and lowest in the 3 °C scenario (Sec. 3.2). The first three processes only occur with interactive atmospheric CO_2 and are the main drivers of the temporal changes in the net ocean capture efficiency. Fourth and fifth, biological activity in the ocean, most prominently calcification, is depending on the ocean state, mostly pH (Orr et al., 2005) and can influence OAE (Lehmann and Bach, 2025). In our Earth system model, calcification responds to changes in the calcite and aragonite saturation states and we find more calcification under OAE than in the reference scenarios. This has two impacts on efficiency: It reduces DIC, allowing for further ocean carbon uptake and increasing efficiency, but also removes alkalinity and thereby decreases efficiency. Both processes lead to a net reduction in efficiency since calcification removes twice as much alkalinity as DIC, leaving a net increase in pCO_2. Calcification however has a small effect on the net efficiency in all scenarios. Overall, before peak atmospheric CO_2, a decline in buffer capacity increases the efficiency of alkalinity-driven CO_2 uptake. However, this gain is largely compensated by ocean outgassing across a larger ocean volume in response to lower atmospheric CO_2, mediated by an additional carbon efflux from the land-biosphere. As a result, net ocean capture efficiency remains nearly constant. Afterwards, as the increase in buffer capacity now reduces

https://doi.org/10.5194/egusphere-2026-255
Preprint. Discussion started: 22 January 2026

efficiency as well, the efficiency generally decreases. The differences in buffer capacity and the land effluxes between warming scenarios balance each other in the long-term, resulting in similar efficiencies between scenarios around 2500.

The gross ocean capture efficiency is close to the maximum ocean capture efficiency, with a mean value of 0.79 [0.78-0.79] in the 2 °C scenario (green line in Fig. 7b). It does not change significantly over time along the emission pathway. By definition, the gross efficiency isolates the direct oceanic response to alkalinity addition, excluding the effects of changes in atmospheric CO_2 due to changes in ocean and land carbon uptake. The gross efficiency is limited by incomplete equilibration following continuous OAE.

The net atmospheric CO_2 reduction efficiency is lower than the net ocean capture efficiency (red lines in Fig. 7), with pre-peak values of 0.52-0.60 with higher efficiencies in the higher warming levels. After peak atmospheric CO_2, efficiencies decline to 0.11-0.12 between 2400 and 2500. The difference between atmospheric CO_2 reduction efficiency and the net ocean capture efficiency arises because the land biosphere releases carbon back to the atmosphere when atmospheric CO_2 levels decline, with larger effluxes in the colder scenarios (Fig. 5). These effluxes are directly accounted for in the net atmospheric reduction efficiency, while also influencing the net ocean capture efficiency indirectly as described above. Variability across individual ensemble members in atmospheric CO_2 reduction efficiency reflects the strong year-to-year variability in land-atmosphere carbon exchange. The near-constant pre-peak efficiencies explain the near-linear reduction of atmospheric CO_2 shown in Fig. 3, with a reducing decrease after peak atmospheric CO_2 as the efficiency drops as well.

To assess the temporal evolution of efficiencies after OAE termination, we extended one ensemble member of the 2°C simulations to the year 3000, terminating OAE in 2500. Since the rate of alkalinity addition is zero after 2500, we evaluate the cumulative efficiency, defined as total carbon uptake divided by total alkalinity addition (Fig. 8). Our results show that the cumulative gross ocean capture efficiency remains below the maximum efficiency over the subsequent 500 years. A persistent ocean-atmosphere pCO_2 difference of approximately 2μatm after OAE termination (not shown) indicates that full equilibration has not yet been achieved. While surface waters continue to equilibrate, previously subducted alkalinity resurfaces through upwelling and mixing, allowing unrealized alkalinity potential to further reduce oceanic pCO_2. In contrast, the cumulative net ocean capture efficiency continues to decrease, as the ocean begins to outgas CO_2 in response to lower atmospheric CO_2 concentrations. Upwelled waters, no longer supported by ongoing alkalinity addition, equilibrate with the reduced atmospheric CO_2 and release carbon. This drives a redistribution of carbon among reservoirs, with the land biosphere taking up carbon again relative to the reference simulation. The net atmospheric CO_2 reduction efficiency decreases further but begins to stabilize, indicating a balance of ocean and land carbon fluxes or a convergence toward a new steady-state carbon balance.

Regional differences in maximum ocean capture efficiency at the surface reflect the sensitivity of surface pCO_2 to alkalinity relative to dissolved inorganic carbon, which is lowest in the tropics and highest at high latitudes ((Fig. C4a). This is consistent with regional differences in the buffer capacity (Egleston et al., 2010). In some regions such as the North Atlantic, North Pacific and parts of the Southern Ocean, gross uptake efficiency locally exceeds the theoretical maximum expected from surface alkalinity addition alone (Fig. C4b). This is due to lateral redistribution of un-equilibrated alkalinity by ocean circulation, which adds local carbon uptake potential and explains the larger than maximum efficiency.

https://doi.org/10.5194/egusphere-2026-255
Preprint. Discussion started: 22 January 2026

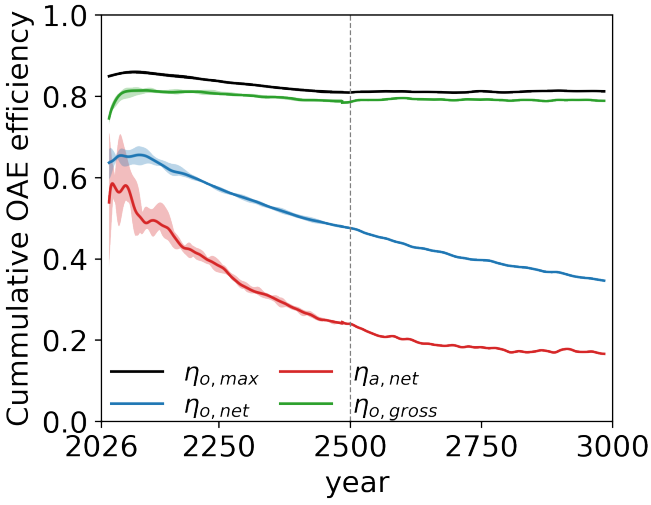

Figure 8. Cumulative efficiencies of ocean alkalinity enhancement; maximum ocean capture efficiency $\eta_{o,max}$ in black, net ocean capture efficiency $\eta_{o,net}$ in blue, net atmospheric CO_2-reduction $\eta_{a,net}$ in red and gross ocean capture efficiency $\eta_{o,gross}$ in green for 2 °C global warming stabilization simulations including the first ensemble member that has been extended until year 3000. All lines are ensemble and 31-year running means, while the shading represents the ensemble spread. OAE termination for the first ensemble member after 2500 is marked with the vertical dashed line.

3.4 Ocean acidification response

The addition of alkalinity leads to a pronounced increase in global mean ocean surface pH relative to the reference scenarios (Fig. 9a). In the absence of alkalinity enhancement (Reference scenarios), global mean surface pH initially declines and subsequently recovers during the global warming stabilization phase, reflecting the initial rise and later decline in atmospheric CO_2. In the OAE scenarios, global mean surface pH during the period 2470 to 2500 is elevated relative to the reference scenario by 0.105 [0.103-0.106] in the 1.5 °C scenario, 0.111 [0.109-0.112] in the 2 °C, and 0.124 [0.123-0.126] in the 3 °C scenario (Fig. 9b). Under the 1.5 °C scenario, this increase is sufficient to raise global mean surface pH above pre-industrial levels, thereby fully reversing historical surface ocean acidification. The temporal evolution of surface pH closely follows that of atmospheric CO_2, with the largest pH changes occurring in the high-warming scenario, where OAE leads to the strongest atmospheric CO_2 drawdown. This is also evident at the regional scale. All regions experience increases in surface pH due to OAE, with slightly larger changes in the 3°C scenario compared to the lower warming scenarios (Fig. C2d-f).

The increase in global surface pH is primarily driven by the reduction in atmospheric CO_2, with smaller additional contributions arise from OAE-specific chemical effects, such as the pH hysteresis and transient pH disequilibrium (Fig. 9; see Sec. 2.4 for further details on the method). In 2100 in the 2°C global warming scenario, the combined effects of pH hysteresis and pCO_2 disequilibrium account for about 48% of the total additional pH increase. Over time, the ocean-atmosphere system progressively equilibrates, and the contribution from atmospheric CO_2 drawdown becomes increasingly dominant, while both the

https://doi.org/10.5194/egusphere-2026-255
Preprint. Discussion started: 22 January 2026

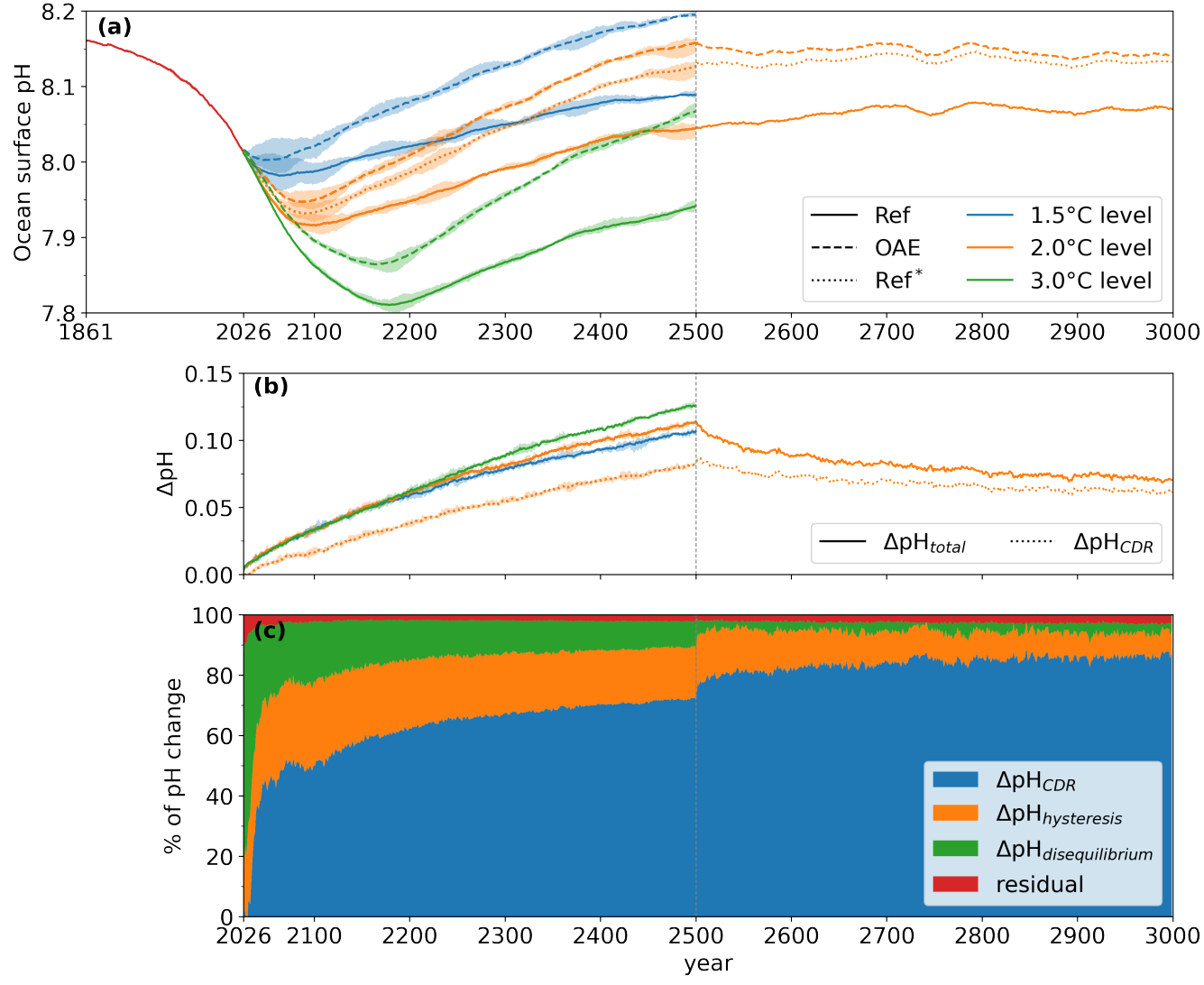

Figure 9. Global ocean surface pH in (a), global surface pH change due to OAE in (b) and contributions to the total global surface pH change due to OAE in (c). Panel (b) shows pH differences between OAE and reference simulations as well as the contribution of the CDR effect. Panel (c) shows the relative contributions from CDR, pH hysteresis , pCO_2 disequilibrium and residual to the total pH change between OAE and reference 2°C simulation. In all panels ensemble means until 2500 are shown and then OAE termination in 2500 for one ensemble member in the 2 °C scenario. Shading in in (a) and (b) indicates ensemble range. Dashed vertical grey lines indicate the timing of OAE termination at year 2500.

https://doi.org/10.5194/egusphere-2026-255
Preprint. Discussion started: 22 January 2026

pH hysteresis and pCO_2 disequilibrium effects diminish. Averaged over 2470 to 2500, approximately 72% of the total global surface pH increase can be attributed to reduced atmospheric CO_2, 17% due to pH hysteresis and 9% due to remaining pCO_2 disequilibrium. The residual is a result of approximations in calculating the three contributions.

Following OAE termination in 2500, the pH difference between the OAE simulation and reference simulation gradually declines (Figure 9b), resulting in a remaining pH response of 0.071 in the year 3000. This reduction in OA mitigation is initially dominated by a decrease in pCO_2 disequilibrium (Figure 9c), as surface waters continue to equilibrate in the decades following termination. However, ongoing upwelling and mixing of previously subducted alkalinity continue to lower oceanic pCO_2, maintaining a nearly constant pCO_2 offset of around 2μatm between the OAE and REF* simulations. Consequently, pCO_2 disequilibrium still explains 2% of the total pH change 500 years after OAE termination. The contribution of the pH hysteresis effect also decreases after 2500, reflecting the declining surface alkalinity difference between the OAE and reference simulations, and accounts for approximately 7% of the pH response in the year 3000. In contrast, while the carbon dioxide removal (CDR) effect weakens after OAE termination (Fig. 9b), its relative importance increases, explaining about 88% of OA mitigation by the year 3000. This weakening of the CDR effect is due to continued outgassing of oceanic CO_2 after OAE termination, driving an increase in atmospheric CO_2 and a decrease in surface ocean pH.

In the subsurface ocean, the largest global mean ocean acidification mitigation from OAE is simulated at a depth of around 250 m, with a maximum pH increase of 0.137 [0.135-0.139] by year 2500 in the 2 °C scenario (Fig. 10a). As at the surface, the subsurface pH mitigation response is larger in the 3 °C scenario and smaller in the 1.5 °C scenario (not shown). The subsurface maximum reflects the competing effects of two opposing vertical gradients: the OAE-induced alkalinity enhancement and associated DIC reduction weakens with depth, whereas the sensitivity of pH to changes in alkalinity and DIC increases with depth. Their combined effect yields a maximum pH response below the surface. Similar subsurface maxima have also been reported for historical ocean acidification (Fassbender et al., 2023; Müller and Gruber, 2024). Consistent with the surface response, pH hysteresis and pCO_2 disequilibrium (Fig. 10c) contribute substantially early on, while CDR effect becomes increasingly dominant over time (Fig. 10b). In 2100, the CDR effect explains 54 % of the total interior pH change, with hysteresis and disequilibrium accounting for the remaining 46 %. By 2500, the CDR contribution increases to 69%. After OAE termination in 2500, the total subsurface pH mitigation gradually declines and the relative contribution of the CDR effect increases to 74% by the year 3000. Below 1000 m, however, pH mitigation continues to increase despite the OAE termination, because ongoing ocean ventilation progressively propagates the accumulated pH deficit into the deep ocean on multi-centennial timescales.

4 Discussion and conclusion

In this study, we assess the efficiency of ocean alkalinity enhancement (OAE), along with its associated climate response and potential to mitigate ocean acidification, under different global warming stabilization scenarios using an emission-driven, comprehensive Earth system model.

https://doi.org/10.5194/egusphere-2026-255
Preprint. Discussion started: 22 January 2026

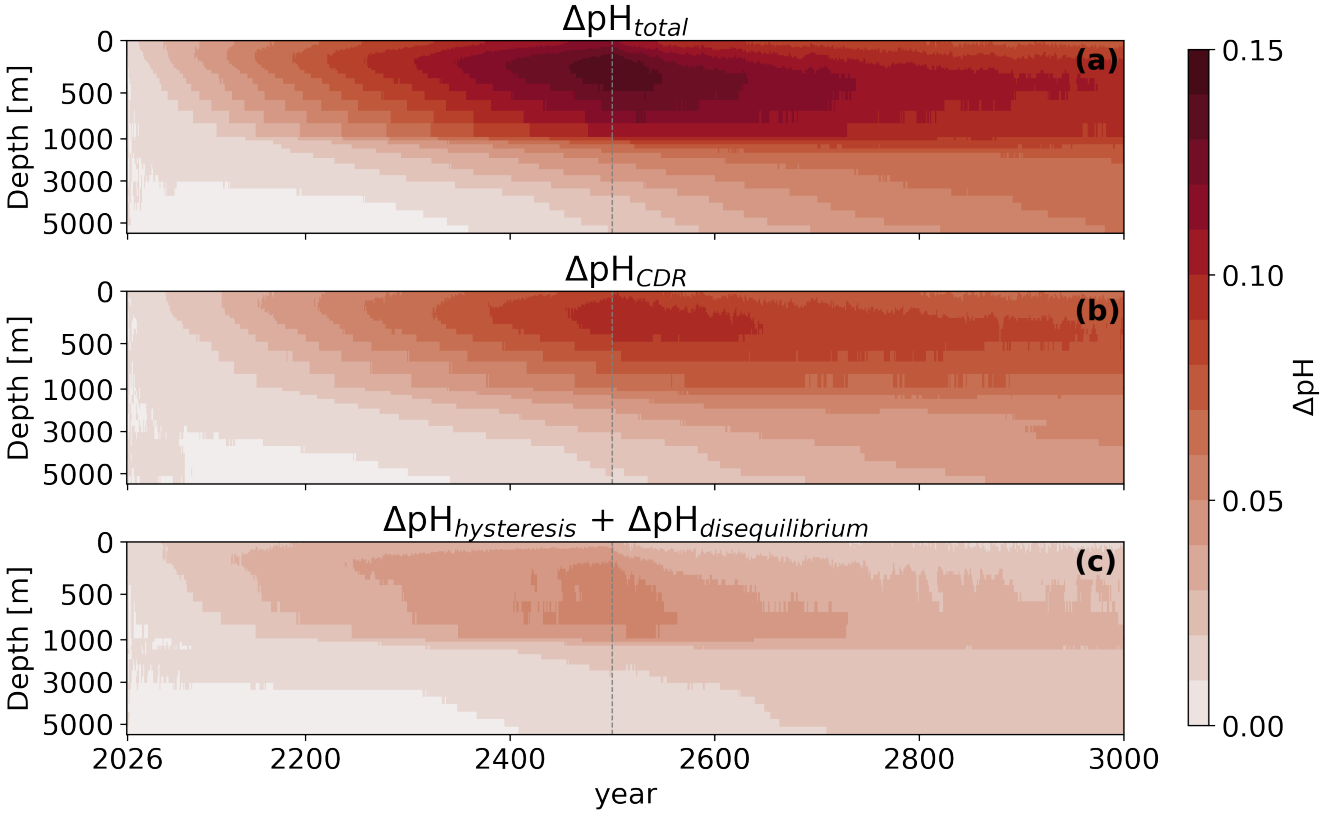

Figure 10. Hovmoeller plots of pH differences due to OAE over depth and time for the 2 °C scenario. The total pH change in (a), the pH response to CDR in (b) and the sum of the pH hysteresis and pCO_2 disequilibrium effects in (c). All plots show the global horizontal averages, ensemble means until 2500 and the first ensemble member with OAE termination after 2500 (vertical dashed line). Note the irregular y-axis, with a break at 1000 m depth.

We find that the global mean surface temperature decreases approximately linearly with continued alkalinity addition, and that the cooling per unit alkalinity added is similar across the three global warming stabilization scenarios. A comparable near-linear temperature response has also been reported by Martin et al. (2025). This suggests that a given amount of alkalinity produces roughly the same cooling effect under both low- and high-warming conditions. Because cumulative CO_2 removal also increases nearly linearly over time, due to an approximately constant, scenario-independent gross ocean capture efficiency, our results imply an approximately linear transient climate response to removal (TCRR) over the range of warming levels explored here (Fig. C5) (Matthews et al., 2009; Zickfeld et al., 2021; Evans and Matthews, 2025) This means that OAE-induced CO_2 removal, diagnosed from gross ocean carbon capture, can be readily incorporated into the well-established TCRE-based framework for estimating remaining carbon budgets consistent with specific temperature targets (Rogelj et al., 2019; Matthews et al., 2020). The near-linearity of the temperature response also indicates that, for OAE, a CDR-tax framework (Boyd et al., 2025) may not be necessary to capture strong state-dependent changes in effectiveness, since the temperature response per unit

https://doi.org/10.5194/egusphere-2026-255
Preprint. Discussion started: 22 January 2026

addition of alkalinity remains approximately constant across the warming levels considered. Nevertheless, the robustness of this result remains to be tested across other Earth system models and experimental setups.

The definition of OAE efficiency strongly influences both its interpretation and policy relevance, as different metrics capture distinct aspects of ocean alkalinity enhancement. The maximum ocean capture efficiency varies between 0.81 and 0.86 when defined at the surface. These moderate variations follow changes in ocean buffer capacity along emission pathways and across global warming scenarios. The gross ocean capture efficiency (about 0.78-0.79 for the 2 °C scenario) quantifies the additional carbon uptake directly induced by OAE and thus reflects its negative emissions potential, making it well suited for carbon accounting and comparison with other CDR approaches such as direct air capture (Tyka, 2025). Similar to the maximum ocean capture efficiency, this metric is also relatively insensitive to the emission pathway. In contrast, the net ocean capture efficiency accounts for Earth system feedbacks that reduce net ocean carbon uptake following atmospheric CO_2 drawdown (Schwinger et al., 2024) and is highly dependent on the climate state. The net atmospheric CO_2 reduction efficiency is further reduced by the CO_2 efflux from the land carbon reservoir and is therefore lower than the net ocean capture efficiency. While the gross efficiency is most appropriate for policy and carbon accounting frameworks, net efficiencies remain essential for assessing long-term carbon storage and climate impacts, such as ocean acidification. Ocean biogeochemical feedbacks in the ocean, such as due to state-dependent calcification rates, affect both gross and net ocean capture efficiencies, consistent with previous studies (Bednaršek et al., 2025; Lehmann and Bach, 2025). These feedbacks are relevant for ocean-only simulations as well, where estimates of gross efficiency can differ depending on whether they are defined as the change in oceanic DIC inventory relative to the change in alkalinity inventory or as the change in air-sea CO_2 flux relative to the added alkalinity, the latter representing negative emissions. In the ESM2M model, the inventory-based efficiency is higher than the flux-based efficiency (Fig. C6) due to enhanced calcification following increasing calcite and aragonite saturation states under the OAE addition. In 2500, inventory-based and flux-based efficiency differ by 0.01 units. Furthermore, the inventory-based efficiency eventually surpasses the maximum ocean capture efficiency calculated at the surface and the full potential of OAE on timescales of millennia is rather limited by the mean ocean maximum efficiency, which is larger with about 0.91. We therefore emphasize that it is essential to clearly specify how efficiencies are calculated and which processes are represented in the applied model, as these choices directly affect policy-relevant efficiency estimates and associated uncertainties.

We show that OAE can mitigate ocean acidification. While surface ocean acidification already reverses in the the global warming stabilization scenarios without OAE due to long-term decline in atmospheric CO_2, OAE provides additional mitigation. Global mean pH in response to OAE increases by 0.11 to 0.12 (1.5 °C scenario to 3 °C scenario) at the surface and by up to 0.13 to 0.15 at subsurface. The majority of this pH increase is driven by the reduction in atmospheric CO_2, a response that is largely independent of the specific CDR approach. In addition, OAE induces direct chemical changes to the ocean carbonate systems, which account for 48% of the surface pH increase after 75 years of OAE and still contribute 27% by the year 2500. Following termination of OAE, these OAE-specific effects diminish over time as the ocean-atmosphere system equilibrates and 88% of surface pH mitigation in the year 3000 comes from reduced atmospheric CO_2. This indicates that emissions reductions remain the most effective and durable strategy for limiting ongoing ocean acidification, and that the long-term acidification mitigation potential provided by OAE is not substantially larger than that achieved through any other CDR approach that

https://doi.org/10.5194/egusphere-2026-255
Preprint. Discussion started: 22 January 2026

lowers atmospheric CO_2, at least on multi-centennial timescales. Although sustained alkalinity addition could, in principle, reduce peak ocean acidification, the required amounts of alkalinity would be immense. At regional and local scales, OAE has the potential to temporarily offset ocean acidification (Albright et al., 2016; Feng et al., 2016; Mongin et al., 2021). However, elevated pH levels, rapid pH changes or the addition of toxic trace metals through impure minerals may also have ecological impacts that remain poorly understood, underscoring the need for caution in deployment and further investigation of biological responses (Feng et al., 2016; Bednaršek et al., 2025; van de Mortel et al., 2025).

Although we consider our conclusions robust, several important caveats must be acknowledged. These relate primarily to (i) the magnitude, spatial distribution, and temporal characteristics of alkalinity deployment, (ii) assumptions regarding the dissolution of added minerals, and (iii) limitations arising from model resolution and simulated biogeochemical complexity. First, the representation of alkalinity addition in our simulations is highly idealized. The total amount of alkalinity applied far exceeds what could be realistically be implemented in the near future (Eisaman et al., 2023), as the amount of needed materials, dependent on the feedstock, corresponds to the current scale of global production (Renforth and Henderson, 2017; Martin et al., 2025), along with substantial infrastructure requiring large investments. Another important point for the readiness of OAE are life cycle emissions, which need emission reductions themselves to make the approach net carbon negative (Foteinis et al., 2022; Delval et al., 2025). Moreover, our simulations assume near global deployment, whereas real-world application would likely be spatially constrained to exclusive economic zones, coastal regions, or shipping corridors (Lezaun, 2021; He and Tyka, 2023). We further assume continuous alkalinity addition, while practical deployment can occur in temporally discrete pulses as well. Nevertheless, continuous alkalinity addition well approximates the alkalinity release from frequent individual pulses necessary for OAE at scale, and continuous addition may also be feasible at specific coastal sites, such as industrial water outlets (Wang et al., 2023; Burt et al., 2024). Consistent with this, we suggest that the large-scale climate and carbon cycle response to a single alkalinity pulse shares the same broad characteristics as the response to continuous OAE. Second, we assume instantaneous dissolution of the added minerals at the ocean surface. Depending on the mineral and grain size, however, dissolution kinetics and particle sinking can substantially delay alkalinity release and reduce near-term carbon uptake efficiency (Köhler et al., 2013; Fakhraee et al., 2023; Burger et al., 2025). More realistic representations of mineral dissolution and particle dynamics are therefore required to better constrain OAE efficiency under plausible deployment scenarios. Third, despite a comparatively realistic representation of alkalinity relative to other Earth system models (Planchat et al., 2023), including explicit aragonite and calcite cycling, several model limitations may influence the simulated OAE response. Notably, the biogeochemical module lacks a more explicit representation of the biological carbon pump, such as particulate organic carbon dynamics, and more detailed sediment-water interactions, both of which could affect long-term carbon and alkalinity cycling. The model also exhibits regional alkalinity biases that may limit its applicability for assessing geographically specific OAE deployments (Dunne et al., 2013). Furthermore, the coarse ocean resolution restricts the representations of mesoscale processes, particularly in western boundary current regions, where we identify strong carbon uptake responses (Guo and Timmermans, 2024). While higher spatial resolution and increased biogeochemical complexity would improve process fidelity, such fully coupled simulations remain computationally prohibitive for the ensemble, multi-centennial simulations across multiple emission scenarios conducted here.

https://doi.org/10.5194/egusphere-2026-255
Preprint. Discussion started: 22 January 2026

In summary, we demonstrate that the net ocean carbon uptake and the resulting atmospheric CO_2 reduction from OAE are modulated by global carbon cycle feedbacks that vary with the emission trajectory. In contrast, the simulated cooling evolves approximately linearly over time, consistent with a near-constant transient climate response to removal (TCRR) under sustained CO_2 drawdown. On centennial timescales, OAE mitigates ocean acidification primarily through reduced atmospheric CO_2; an effect common to other CDR approaches. Direct chemical pH increase from added alkalinity is most important during the first decades and becomes progressively less important thereafter. Overall, these results underscore that rapid emission reductions remain the most effective strategy for achieving the Paris Agreement goals and mitigating ocean acidification.

https://doi.org/10.5194/egusphere-2026-255
Preprint. Discussion started: 22 January 2026

Appendix A: Equivalence of OAE and direct air capture in reducing atmospheric CO_2

We investigate whether OAE in an emission-driven framework leads to the same reduction in atmospheric CO_2 as would be obtained by applying the additional ocean carbon uptake diagnosed from a concentration-driven OAE simulation as negative emissions in an emission driven simulation (i.e. equivalent to direct air capture DAC). This analysis reassesses the findings of Tyka (2025) using a fully coupled Earth system model. The additional carbon uptake is equivalent to the gross ocean carbon capture, which is also quantified by the gross ocean capture efficiency.

To test this, we performed a set of 200-yr pre-industrial simulations (Fig. A1): (i) an emission-driven control simulation with zero emissions (red line), (ii) a concentration-driven simulation with atmospheric CO_2 fixed at 286 ppm and no OAE (orange line), (iii) a concentration-driven simulation with atmospheric CO_2 fixed at 286 ppm and continuous OAE applied using the same forcing as described in Sec. 2.2 (blue line), (iv) an emission-driven simulation in which the difference in ocean carbon uptake between simulations (ii) and (iii) is imposed as a negative emission forcing, directly removing carbon from the atmospheric reservoir and the global carbon cycle can react to the changes in atmospheric CO_2 (purple line), and (v) an emission-driven simulation with zero emissions, but with OAE applied identically to simulation (iii) (green line).

The emission-driven simulations with negative emissions (purple) and with OAE (green) exhibit nearly identical reductions in atmospheric CO_2 supporting the findings of Tyka (2025). The small difference may be explained by internal variability, which is on the same order as in the control (red). This result demonstrates that carbon cycle feedbacks respond equivalently to CO_2 removal from the atmosphere and to additional ocean carbon uptake induced by OAE. Therefore, concentration-driven ocean-only model simulations with and without OAE are sufficient to quantify the expected carbon removal from OAE, hence the gross ocean capture efficiency, and to inform carbon accounting and crediting frameworks (Tyka, 2025). Fully coupled Earth system models, however, remain essential for assessing the broader climate response.

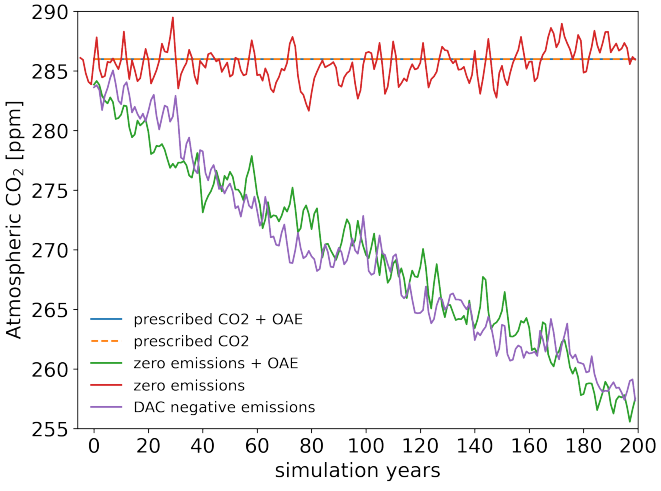

Figure A1. Simulated atmospheric CO_2 concentrations in a set of pre-industrial simulations. Details are explained in Appendix A.

https://doi.org/10.5194/egusphere-2026-255
Preprint. Discussion started: 22 January 2026

Appendix B: Derivation of the pH hysteresis effect

The ocean carbonate system is governed by the equilibrium constants relating oceanic partial pressure of CO_2 (pCO_2), carbonic acid ($[H_2CO_3{}^*]$), bicarbonate ($[HCO_3^-]$), carbonate ions ($[CO_3^{2-}]$), and protons ([H$^+$]):

$$K_0 = \frac{[H_2CO_3{}^*]}{pCO_2}, \quad K_1 = \frac{[H^+][HCO_3^-]}{[H_2CO_3{}^*]}, \quad K_2 = \frac{[H^+][CO_3^{2-}]}{[HCO_3^-]}.$$

Combining these expressions yields two equivalent formulations for pCO_2:

$$pCO_2 = \frac{[H^+][HCO_3^-]}{K_0 K_1} \quad \text{and} \quad pCO_2 = \frac{[H^+]^2[CO_3^{2-}]}{K_0 K_1 K_2}.$$

We assume that alkalinity addition induces a change in pCO_2 that fully equilibrates with the atmosphere, such that the pCO_2 remains unchanged before and after equilibration:

$$pCO_2{}^{start} = pCO_2{}^{end}. \tag{B1}$$

This implies

$$[H^+]^{start}[HCO_3^-]^{start} = [H^+]^{end}[HCO_3^-]^{end} \tag{B2}$$

and

$$([H^+]^{start})^2[CO_3^{2-}]^{start} = ([H^+]^{end})^2[CO_3^{2-}]^{end}. \tag{B3}$$

Uptake of atmospheric CO_2 by the ocean predominantly increases the bicarbonate concentration ($[HCO_3^-]$) (Orr et al., 2005). We therefore introduce a small parameter $\epsilon \ll 1$ describing the relative increase in bicarbonate during equilibration:

$$\frac{[HCO_3^-]^{\text{end}}}{[HCO_3^-]^{\text{start}}} = 1 + \epsilon. \tag{B4}$$

Combining Eqs. B2, B3 and B4 yields

$$\frac{[CO_3^{2-}]^{\text{end}}}{[CO_3^{2-}]^{\text{start}}} = (1+\epsilon)^2. \tag{B5}$$

The total change in dissolved inorganic carbon (ΔDIC) due to OAE is given by the change in bicarbonate and carbonate concentrations:

$$\Delta\text{DIC} = [HCO_3^-]^{\text{end}} + [CO_3^{2-}]^{\text{end}} - [HCO_3^-]^{\text{start}} - [CO_3^{2-}]^{\text{start}}. \tag{B6}$$

By using Eqs. B4 and B5, this yields

$$\Delta\text{DIC} = \epsilon[HCO_3^-]^{\text{start}} + (2\epsilon + \epsilon^2)[CO_3^{2-}]^{\text{start}}. \tag{B7}$$

https://doi.org/10.5194/egusphere-2026-255
Preprint. Discussion started: 22 January 2026

Since ΔDIC is positive for OAE, ϵ is positive as well and assuming that $\epsilon^2 \approx 0$ since $\epsilon \ll 1$, this simplifies to

$$\Delta\text{DIC} = \epsilon \left([HCO_3^-]^{\text{start}} + 2[CO_3^{2-}]^{\text{start}} \right). \tag{B8}$$

The bracket in equation B8 describes the contribution of bicarbonate and carbonate ions to alkalinity. As bicarbonate and carbonate ions makes up about 96 % of the alkalinity in the ocean (Sarmiento and Gruber, 2006), we assume this to be the total alkalinity of the ocean before alkalinity addition, i.e. the alkalinity in the reference simulation (ALK^{Ref}). Equation B8 can therefore be written as:

$$\Delta DIC = \epsilon\, ALK^{Ref}. \tag{B9}$$

As discussed in Section 2.3.3, under perfect equilibration, the total additional DIC change is proportional to the added alkalinity, with the proportionality given by the maximum ocean capture efficiency $\eta_{o,max}$:

$$\Delta DIC = \eta_{o,max} \Delta ALK. \tag{B10}$$

Using Eqs. B9 and B10, we can write ϵ as

$$\epsilon = \eta_{o,max} \frac{\Delta ALK}{ALK^{Ref}}. \tag{B11}$$

To quantify the pH after equilibration, we combine Eqs. B2 and B4 and get the amount of protons after equilibration:

$$[H^+]^{end} = \frac{1}{1+\epsilon} [H^+]^{start}. \tag{B12}$$

And since $pH = -log_{10}([H^+])$, the pH after equilibration can be calculated as:

$$pH^{end} = log_{10}(1+\epsilon) + pH^{start}. \tag{B13}$$

Since $\epsilon \ll 1$, we can approximate $log_{10}(1+\epsilon) \approx \epsilon \frac{1}{ln(10)}$, and the pH hysteresis effect is approximated by

$$\Delta pH_{hysteresis} = pH^{end} - pH^{start} = \eta_{o,max} \frac{\Delta ALK}{ALK^{Ref}} \frac{1}{ln(10)} \tag{B14}$$

https://doi.org/10.5194/egusphere-2026-255
Preprint. Discussion started: 22 January 2026

Appendix C: Supplementary Figures

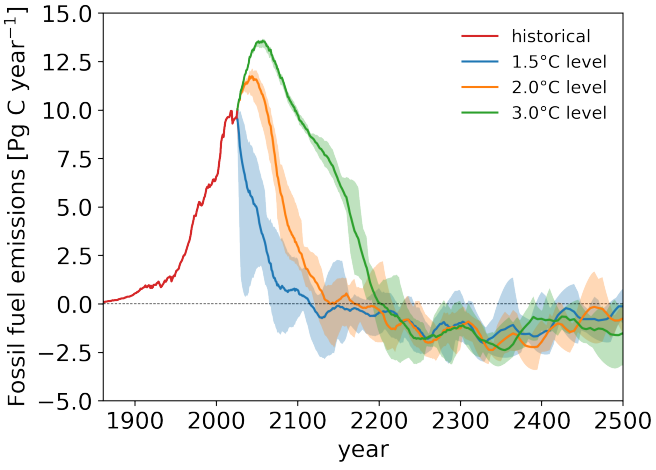

Figure C1. Emission trajectories from the adaptive emission reduction approach to stabilise at global warming levels of 1.5, 2.0 and 3.0 °C. All lines are ensemble means, while the shading represents the ensemble range.

https://doi.org/10.5194/egusphere-2026-255
Preprint. Discussion started: 22 January 2026

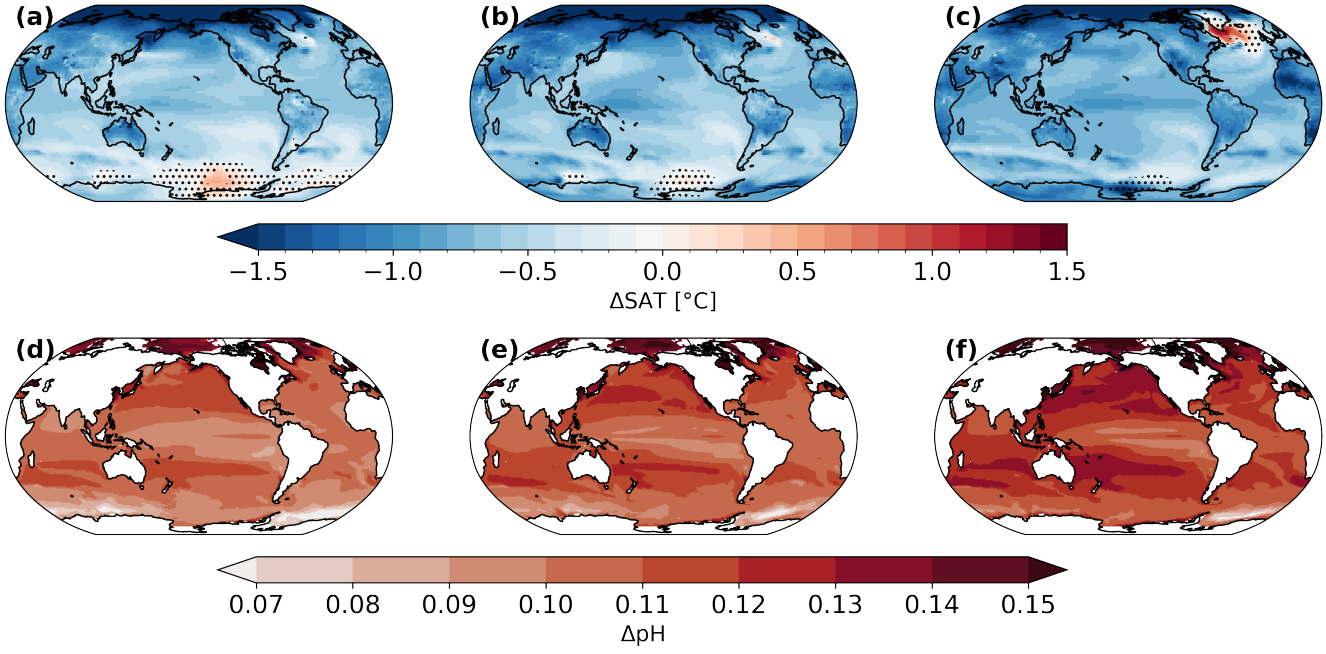

Figure C2. Regional patterns of surface air temperature (a-c) and surface pH (d-f) changes between the OAE and the reference simulation for the period of 2470-2500 for the 1.5 °C level (a,d), the 2 °C level (b,e) and the 3 °C level (c,f). Regions without hatching show significance at the 95% level based on a two-sided students t-test.

https://doi.org/10.5194/egusphere-2026-255
Preprint. Discussion started: 22 January 2026

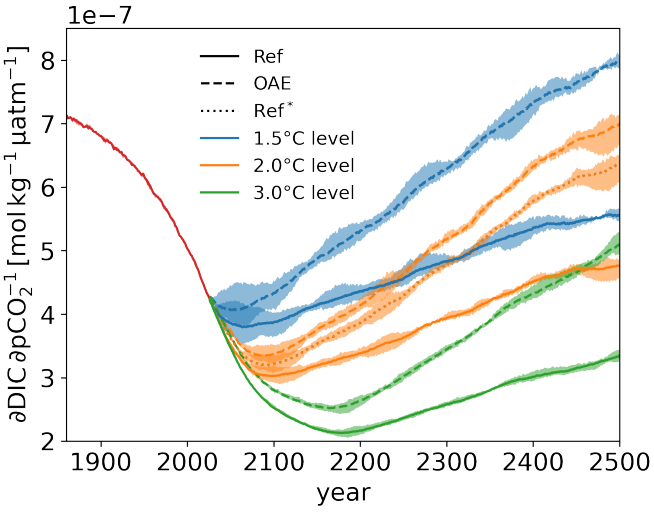

Figure C3. The global ocean buffer capacity from 1861 until 2500 for the different global warming scenarios with and without OAE. Lines are the five member ensemble mean and shading refers to the ensemble range. A low buffer capacity represents a high sensitivity of pCO_2 to DIC and a high Revelle factor and vice versa (Revelle and Suess, 1957).

https://doi.org/10.5194/egusphere-2026-255
Preprint. Discussion started: 22 January 2026

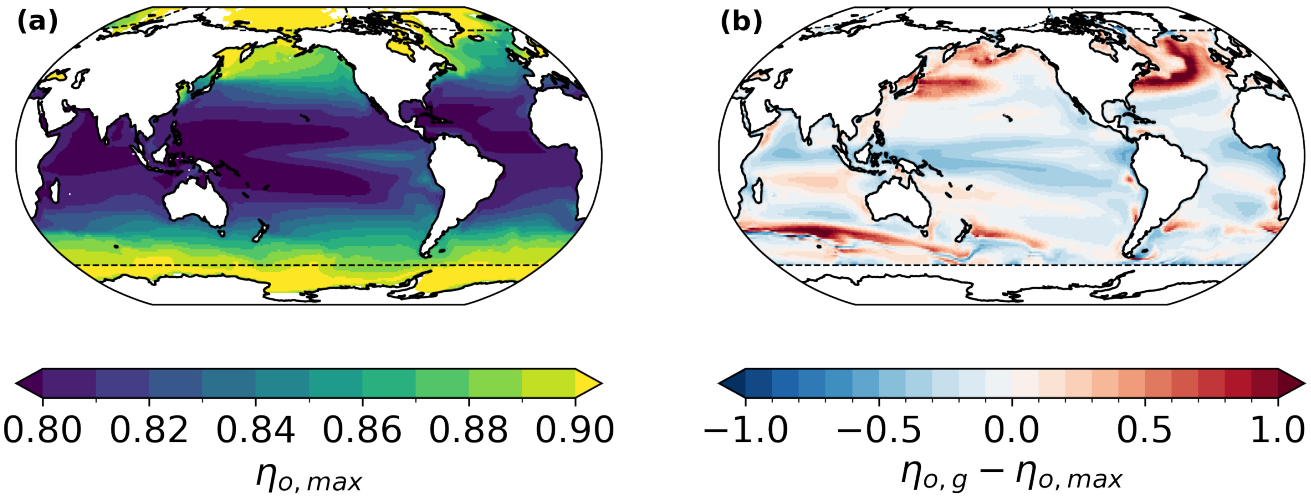

Figure C4. Spatial pattern of the maximum ocean capture efficiency (b) and the difference between the gross ocean capture efficiency and the maximum ocean capture efficiency (b), averaged over 2026 and 2500.

https://doi.org/10.5194/egusphere-2026-255
Preprint. Discussion started: 22 January 2026

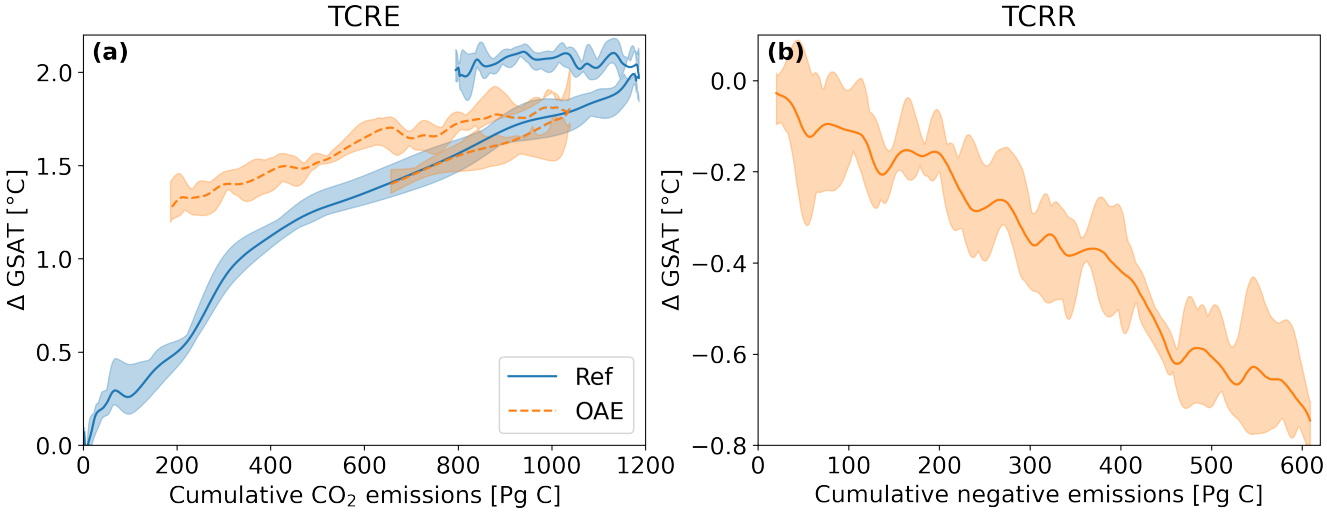

Figure C5. Simulated transient climate response to cumulative CO_2 emissions (TCRE) in (a) and transient climate response to removal (TCRR) in (b). Panel (a) show TCRE for the reference simulation (Ref) and the global surface air temperature response to the total positive fossil fuel emissions plus negative emissions due to OAE (OAE). Panel (b) shows the TCRR as the temperature difference between OAE and the reference simulation against the cumulative negative CO_2 emissions resulting from the gross carbon capture efficiency. The figure only shows the 2 °C scenario, since the Ref* simulations are necessary to calculate negative emissions. All lines are ensemble and 31-year running means, while the shading represents the ensemble spread.

https://doi.org/10.5194/egusphere-2026-255
Preprint. Discussion started: 22 January 2026

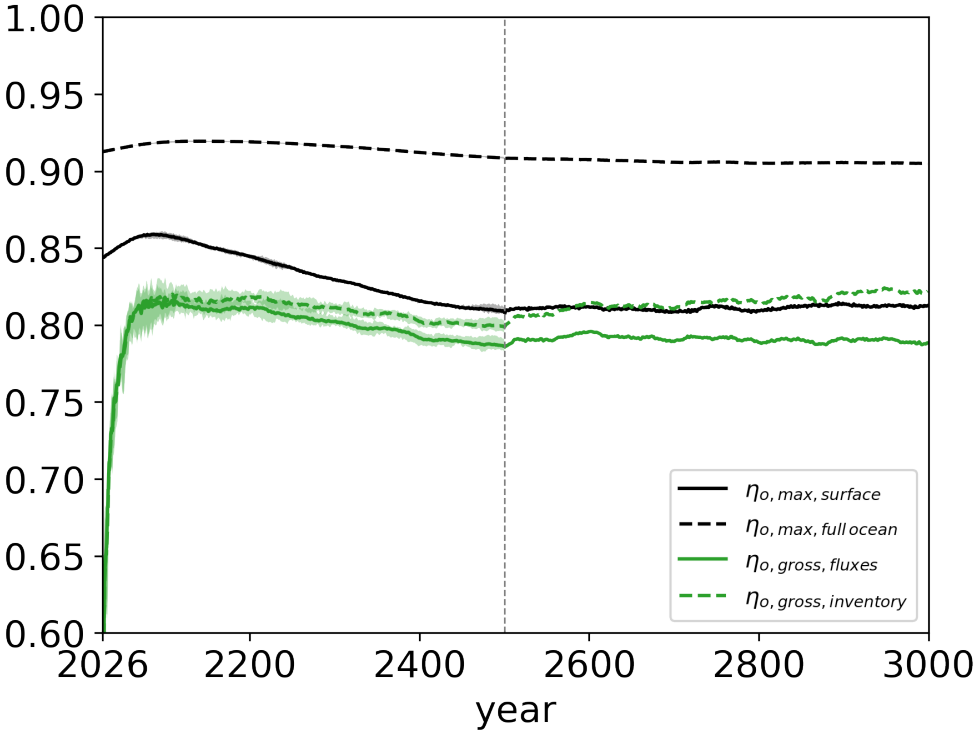

Figure C6. Cumulative efficiencies of ocean alkalinity enhancement; maximum ocean capture efficiency $\eta_{o,max}$ in black and gross ocean capture efficiency $\eta_{o,gross}$ in green for the 2 °C global warming scenario. Surface maximum efficiency and gross efficiency from air-sea CO_2 fluxes in the solid lines, average maximum efficiency for the full ocean and gross efficiencies from DIC and alkalinity inventory changes in the dashed lines. All lines are ensemble means, while the shading represents the ensemble spread. OAE termination for the first ensemble member after 2500 is marked with the vertical dashed line.

https://doi.org/10.5194/egusphere-2026-255
Preprint. Discussion started: 22 January 2026

Code and data availability. Code and Data to reproduce figures is available here: https://gitlab.climate.unibe.ch/hendrik.grosselindemann/the-efficiency-and-ocean-acidification-mitigation-potential-of-ocean-alkalinity-enhancement-on-multi-centennial-timescales.git. It will be uploaded to and assigned a DOI on Zenodo upon publication.

Author contributions. All authors designed the study. HG ran the simulations with OAE and the additional reference simulations under prescribed CO_2, analysed the model output and wrote the initial manuscript draft. FAB contributed significantly to the development of theoretical frameworks to explain processes and ran the reference simulations. TLF acquired funding. All authors discussed results and contributed to revising, editing, and writing of the paper.

Competing interests. The authors declare no competing interests.

Acknowledgements. This work was supported by the Bloom Foundation. The authors also thank the CSCS Swiss National Supercomputing Centre for computing resources (project number s1328) and Raffaele Bernardello for initial discussions.

https://doi.org/10.5194/egusphere-2026-255
Preprint. Discussion started: 22 January 2026

References

Albright, R., Caldeira, L., Hosfelt, J., Kwiatkowski, L., Maclaren, J. K., Mason, B. M., Nebuchina, Y., Ninokawa, A., Pongratz, J., Ricke, K. L., Rivlin, T., Schneider, K., Sesboüé, M., Shamberger, K., Silverman, J., Wolfe, K., Zhu, K., and Caldeira, K.: Reversal of ocean acidification enhances net coral reef calcification, Nature, 531, 362–365, https://doi.org/10.1038/nature17155, 2016.

Anderson, Jeffrey L., Balaji, V., Broccoli, Anthony J., Cooke, William F., Delworth, Thomas L., Dixon, Keith W., Donner, Leo J., Dunne, Krista A., Freidenreich, Stuart M., Garner, Stephen T., Gudgel, Richard G., Gordon, C. T., Held, Isaac M., Hemler, Richard S., Horowitz, Larry W., Klein, Stephen A., Knutson, Thomas R., Kushner, Paul J., Langenhost, Amy R., Lau, Ngar-Cheung, Liang, Zhi, Malyshev, Sergey L., Milly, P. C. D., Nath, Mary J., Ploshay, Jeffrey J., Ramaswamy, V., Schwarzkopf, M. Daniel, Shevliakova, Elena, Sirutis, Joseph J., Soden, Brian J., Stern, William F., Thompson, Lori A., Wilson, R. John, Wittenberg, Andrew T., and Wyman, Bruce L.: The New GFDL Global Atmosphere and Land Model AM2–LM2: Evaluation with Prescribed SST Simulations, Journal of Climate, 17, 4641–4673, https://doi.org/10.1175/JCLI-3223.1, 2004.

Bach, L. T., Gill, S. J., Rickaby, R. E. M., Gore, S., and Renforth, P.: CO2 Removal With Enhanced Weathering and Ocean Alkalinity Enhancement: Potential Risks and Co-benefits for Marine Pelagic Ecosystems, Frontiers in Climate, 1, 7, https://doi.org/10.3389/fclim.2019.00007, 2019.

Bednaršek, N., van de Mortel, H., Pelletier, G., García-Reyes, M., Feely, R. A., and Dickson, A. G.: Assessment framework to predict sensitivity of marine calcifiers to ocean alkalinity enhancement – identification of biological thresholds and importance of precautionary principle, Biogeosciences, 22, 473–498, https://doi.org/10.5194/bg-22-473-2025, 2025.

Boehm, S., Jeffery, L., Hecke, J., Schumer, C., Jaeger, J., Fyson, C., Levin, K., Nilsson, A., Naimoli, S., Daly, E., Thwaites, J., Lebling, K., Waite, R., Collis, J., Sims, M., Singh, N., Grier, E., Lamb, W., Castellanos, S., Lee, A., Geffray, M.-C., Santo, R., Balehegn, M., Petroni, M., and Masterson, M.: State of Climate Action 2023, World Resources Institute, https://doi.org/10.46830/wrirpt.23.00010, 2023.

Bopp, L., Resplandy, L., Orr, J. C., Doney, S. C., Dunne, J. P., Gehlen, M., Halloran, P., Heinze, C., Ilyina, T., Séférian, R., Tjiputra, J., and Vichi, M.: Multiple stressors of ocean ecosystems in the 21st century: projections with CMIP5 models, Biogeosciences, 10, 6225–6245, https://doi.org/10.5194/bg-10-6225-2013, 2013.

Bossy, T., Ciais, P., Tanaka, K., Lecocq, F., Bousquet, P., and Gasser, T.: Spaces of anthropogenic CO2 emissions compatible with climate boundaries, Nature Climate Change, pp. 1–8, https://doi.org/10.1038/s41558-025-02460-5, 2025.

Boyd, P. W., Gattuso, J.-P., Legendre, L., Moustakis, Y., and Pongratz, J.: Effective carbon dioxide removal requires a One-Earth approach, Environmental Research Letters, 20, 111 004, https://doi.org/10.1088/1748-9326/ae15a8, 2025.

Bronselaer, B., Winton, M., Russell, J., Sabine, C. L., and Khatiwala, S.: Agreement of CMIP5 Simulated and Observed Ocean Anthropogenic CO2 Uptake, Geophysical Research Letters, 44, 12,298–12,305, https://doi.org/10.1002/2017GL074435, 2017.

Burger, F. A., John, J. G., and Frölicher, T. L.: Increase in ocean acidity variability and extremes under increasing atmospheric CO_2, Biogeosciences, 17, 4633–4662, https://doi.org/10.5194/bg-17-4633-2020, 2020.

Burger, F. A., Terhaar, J., and Frölicher, T. L.: Compound marine heatwaves and ocean acidity extremes, Nature Communications, 13, 4722, https://doi.org/10.1038/s41467-022-32120-7, 2022.

Burger, F. A., Hofmann Elizondo, U., Grosselindemann, H., and Frölicher, T. L.: Subsurface dissolution reduces the efficiency of mineral-based ocean alkalinity enhancement, EGUsphere, pp. 1–27, https://doi.org/10.5194/egusphere-2025-5917, 2025.

https://doi.org/10.5194/egusphere-2026-255
Preprint. Discussion started: 22 January 2026

Burt, W., Rackley, S., Izett, R., Vallis, J., Sadoon, O., Rau, G., Melashvili, M., and Cross, T.: Planetary Technologies' Groundbreaking Marine Carbon Dioxide Removal (mCDR) Project in Halifax, and the Emergence of Halifax as a Global mCDR Hub, in: OCEANS 2024 - Halifax, pp. 1–6, https://doi.org/10.1109/OCEANS55160.2024.10754096, 2024.

Butenschön, M., Lovato, T., Masina, S., Caserini, S., and Grosso, M.: Alkalinization Scenarios in the Mediterranean Sea for Efficient Removal of Atmospheric CO2 and the Mitigation of Ocean Acidification, Frontiers in Climate, 3, https://doi.org/10.3389/fclim.2021.614537, 2021.

Delval, M. H., Thonemann, N., Henriksson, P. J. G., Tanzer, S. E., and Behrens, P.: Life cycle assessment of ocean-based carbon dioxide removal approaches: A systematic literature review, Renewable and Sustainable Energy Reviews, 224, 116 091, https://doi.org/10.1016/j.rser.2025.116091, 2025.

Deser, C., Lehner, F., Rodgers, K. B., Ault, T., Delworth, T. L., DiNezio, P. N., Fiore, A., Frankignoul, C., Fyfe, J. C., Horton, D. E., Kay, J. E., Knutti, R., Lovenduski, N. S., Marotzke, J., McKinnon, K. A., Minobe, S., Randerson, J., Screen, J. A., Simpson, I. R., and Ting, M.: Insights from Earth system model initial-condition large ensembles and future prospects, Nature Climate Change, 10, 277–286, https://doi.org/10.1038/s41558-020-0731-2, 2020.

Doney, S. C., Fabry, V. J., Feely, R. A., and Kleypas, J. A.: Ocean Acidification: The Other CO2 Problem, Annual Review of Marine Science, 1, 169–192, https://doi.org/10.1146/annurev.marine.010908.163834, 2009.

Doney, S. C., Wolfe, W. H., McKee, D. C., and Fuhrman, J. G.: The Science, Engineering, and Validation of Marine Carbon Dioxide Removal and Storage, Annual Review of Marine Science, 17, 55–81, https://doi.org/10.1146/annurev-marine-040523-014702, 2025.

Dunne, J. P., John, J. G., Adcroft, A. J., Griffies, S. M., Hallberg, R. W., Shevliakova, E., Stouffer, R. J., Cooke, W., Dunne, K. A., Harrison, M. J., Krasting, J. P., Malyshev, S. L., Milly, P. C. D., Phillipps, P. J., Sentman, L. T., Samuels, B. L., Spelman, M. J., Winton, M., Wittenberg, A. T., and Zadeh, N.: GFDL's ESM2 Global Coupled Climate–Carbon Earth System Models. Part I: Physical Formulation and Baseline Simulation Characteristics, Journal of Climate, 25, 6646–6665, https://doi.org/10.1175/JCLI-D-11-00560.1, 2012.

Dunne, J. P., John, J. G., Shevliakova, E., Stouffer, R. J., Krasting, J. P., Malyshev, S. L., Milly, P. C. D., Sentman, L. T., Adcroft, A. J., Cooke, W., Dunne, K. A., Griffies, S. M., Hallberg, R. W., Harrison, M. J., Levy, H., Wittenberg, A. T., Phillips, P. J., and Zadeh, N.: GFDL's ESM2 Global Coupled Climate–Carbon Earth System Models. Part II: Carbon System Formulation and Baseline Simulation Characteristics*, Journal of Climate, 26, 2247–2267, https://doi.org/10.1175/JCLI-D-12-00150.1, 2013.

Egleston, E. S., Sabine, C. L., and Morel, F. M. M.: Revelle revisited: Buffer factors that quantify the response of ocean chemistry to changes in DIC and alkalinity, Global Biogeochemical Cycles, 24, https://doi.org/10.1029/2008GB003407, 2010.

Eisaman, M. D., Geilert, S., Renforth, P., Bastianini, L., Campbell, J., Dale, A. W., Foteinis, S., Grasse, P., Hawrot, O., Löscher, C. R., Rau, G. H., and Rønning, J.: Assessing the technical aspects of ocean-alkalinity-enhancement approaches, State of the Planet, 2-oae2023, 1–29, https://doi.org/10.5194/sp-2-oae2023-3-2023, 2023.

Evans, R. C. and Matthews, H. D.: The effectiveness of agricultural carbon dioxide removal using the University of Victoria Earth System Climate Model, Biogeosciences, 22, 1969–1984, https://doi.org/10.5194/bg-22-1969-2025, 2025.

Fakhraee, M., Li, Z., Planavsky, N. J., and Reinhard, C. T.: A biogeochemical model of mineral-based ocean alkalinity enhancement: impacts on the biological pump and ocean carbon uptake, Environmental Research Letters, 18, 044 047, https://doi.org/10.1088/1748-9326/acc9d4, 2023.

Fassbender, A. J., Carter, B. R., Sharp, J. D., Huang, Y., Arroyo, M. C., and Frenzel, H.: Amplified Subsurface Signals of Ocean Acidification, Global Biogeochemical Cycles, 37, e2023GB007 843, https://doi.org/10.1029/2023GB007843, 2023.

Feng, E. Y., Keller, D. P., Koeve, W., and Oschlies, A.: Could artificial ocean alkalinization protect tropical coral ecosystems from ocean acidification?, Environmental Research Letters, 11, 074 008, https://doi.org/10.1088/1748-9326/11/7/074008, 2016.

https://doi.org/10.5194/egusphere-2026-255
Preprint. Discussion started: 22 January 2026

Fennel, K., Long, M. C., Algar, C., Carter, B., Keller, D., Laurent, A., Mattern, J. P., Musgrave, R., Oschlies, A., Ostiguy, J., Palter, J. B., and Whitt, D. B.: Modelling considerations for research on ocean alkalinity enhancement (OAE), State of the Planet, 2-oae2023, 9, https://doi.org/10.5194/sp-2-oae2023-9-2023, publication title: Guide to best practices in ocean alkalinity enhancement research Publisher: Copernicus Publications, 2023.

Findlay, H. S., Feely, R. A., Grabb, K., Jewett, E. B., and Keister, E. F.: FEATURE ARTICLE • Perspectives on Marine Carbon Dioxide Removal from the Global Ocean Acidification Observing Network, Oceanography, 38, 24–39, https://doi.org/10.5670/oceanog.2025.e308, 2025.

Forster, P. M., Smith, C., Walsh, T., Lamb, W. F., Lamboll, R., Cassou, C., Hauser, M., Hausfather, Z., Lee, J.-Y., Palmer, M. D., Von Schuckmann, K., Slangen, A. B. A., Szopa, S., Trewin, B., Yun, J., Gillett, N. P., Jenkins, S., Matthews, H. D., Raghavan, K., Ribes, A., Rogelj, J., Rosen, D., Zhang, X., Allen, M., Aleluia Reis, L., Andrew, R. M., Betts, R. A., Borger, A., Broersma, J. A., Burgess, S. N., Cheng, L., Friedlingstein, P., Domingues, C. M., Gambarini, M., Gasser, T., Gütschow, J., Ishii, M., Kadow, C., Kennedy, J., Killick, R. E., Krummel, P. B., Liné, A., Monselesan, D. P., Morice, C., Mühle, J., Naik, V., Peters, G. P., Pirani, A., Pongratz, J., Minx, J. C., Rigby, M., Rohde, R., Savita, A., Seneviratne, S. I., Thorne, P., Wells, C., Western, L. M., Van Der Werf, G. R., Wijffels, S. E., Masson-Delmotte, V., and Zhai, P.: Indicators of Global Climate Change 2024: annual update of key indicators of the state of the climate system and human influence, Earth System Science Data, 17, 2641–2680, https://doi.org/10.5194/essd-17-2641-2025, 2025.

Foteinis, S., Andresen, J., Campo, F., Caserini, S., and Renforth, P.: Life cycle assessment of ocean liming for carbon dioxide removal from the atmosphere, Journal of Cleaner Production, 370, 133 309, https://doi.org/10.1016/j.jclepro.2022.133309, 2022.

Frankignoulle, M., Canon, C., and Gattuso, J.: Marine calcification as a source of carbon dioxide: Positive feedback of increasing atmospheric CO_2, Limnology and Oceanography, 39, 458–462, https://doi.org/10.4319/lo.1994.39.2.0458, 1994.

Friedlingstein, P., O'Sullivan, M., Jones, M. W., Andrew, R. M., Bakker, D. C. E., Hauck, J., Landschützer, P., Le Quéré, C., Li, H., Luijkx, I. T., Peters, G. P., Peters, W., Pongratz, J., Schwingshackl, C., Sitch, S., Canadell, J. G., Ciais, P., Aas, K., Alin, S. R., Anthoni, P., Barbero, L., Bates, N. R., Bellouin, N., Benoit-Cattin, A., Berghoff, C. F., Bernardello, R., Bopp, L., Brasika, I. B. M., Chamberlain, M. A., Chandra, N., Chevallier, F., Chini, L. P., Collier, N. O., Colligan, T. H., Cronin, M., Djeutchouang, L., Dou, X., Enright, M. P., Enyo, K., Erb, M., Evans, W., Feely, R. A., Feng, L., Ford, D. J., Foster, A., Fransner, F., Gasser, T., Gehlen, M., Gkritzalis, T., Goncalves De Souza, J., Grassi, G., Gregor, L., Gruber, N., Guenet, B., Gürses, O., Harrington, K., Harris, I., Heinke, J., Hurtt, G. C., Iida, Y., Ilyina, T., Ito, A., Jacobson, A. R., Jain, A. K., Jarníková, T., Jersild, A., Jiang, F., Jones, S. D., Kato, E., Keeling, R. F., Klein Goldewijk, K., Knauer, J., Kong, Y., Korsbakken, J. I., Koven, C., Kunimitsu, T., Lan, X., Liu, J., Liu, Z., Liu, Z., Lo Monaco, C., Ma, L., Marland, G., McGuire, P. C., McKinley, G. A., Melton, J., Monacci, N., Monier, E., Morgan, E. J., Munro, D. R., Müller, J. D., Nakaoka, S.-I., Nayagam, L. R., Niwa, Y., Nutzel, T., Olsen, A., Omar, A. M., Pan, N., Pandey, S., Pierrot, D., Qin, Z., Regnier, P. A. G., Rehder, G., Resplandy, L., Roobaert, A., Rosan, T. M., Rödenbeck, C., Schwinger, J., Skjelvan, I., Smallman, T. L., Spada, V., Sreeush, M. G., Sun, Q., Sutton, A. J., Sweeney, C., Swingedouw, D., Séférian, R., Takao, S., Tatebe, H., Tian, H., Tian, X., Tilbrook, B., Tsujino, H., Tubiello, F., Van Ooijen, E., Van Der Werf, G., Van De Velde, S. J., Walker, A., Wanninkhof, R., Yang, X., Yuan, W., Yue, X., and Zeng, J.: Global Carbon Budget 2025, https://doi.org/10.5194/essd-2025-659, 2025.

Frölicher, T. L. and Paynter, D. J.: Extending the relationship between global warming and cumulative carbon emissions to multi-millennial timescales, Environmental Research Letters, 10, 075 002, https://doi.org/10.1088/1748-9326/10/7/075002, 2015.

Frölicher, T. L., Joos, F., Plattner, G.-K., Steinacher, M., and Doney, S. C.: Natural variability and anthropogenic trends in oceanic oxygen in a coupled carbon cycle–climate model ensemble, Global Biogeochemical Cycles, 23, https://doi.org/10.1029/2008GB003316, 2009.

https://doi.org/10.5194/egusphere-2026-255
Preprint. Discussion started: 22 January 2026

675 Frölicher, T. L., Winton, M., and Sarmiento, J. L.: Continued global warming after CO2 emissions stoppage, Nature Climate Change, 4, 40–44, https://doi.org/10.1038/nclimate2060, 2014.

Frölicher, T. L., Sarmiento, J. L., Paynter, D. J., Dunne, J. P., Krasting, J. P., and Winton, M.: Dominance of the Southern Ocean in Anthropogenic Carbon and Heat Uptake in CMIP5 Models, Journal of Climate, https://doi.org/10.1175/JCLI-D-14-00117.1, 2015.

Frölicher, T. L., Fischer, E. M., and Gruber, N.: Marine heatwaves under global warming, Nature, 560, 360–364,
680 https://doi.org/10.1038/s41586-018-0383-9, 2018.

Frölicher, T. L., Ramseyer, L., Raible, C. C., Rodgers, K. B., and Dunne, J.: Potential predictability of marine ecosystem drivers, Biogeosciences, 17, 2061–2083, https://doi.org/10.5194/bg-17-2061-2020, 2020.

Griffies, S. M., NOAA, and Laboratory, G. F. D.: ELEMENTS OF MOM4P1, GFDL OCEAN GROUP TECHNICAL REPORT NO. 6, https://doi.org/https://www.gfdl.noaa.gov/wp-content/uploads/files/model_development/ocean/guide4p1.pdf, 2009.

685 Guo, Y. and Timmermans, M.-L.: The Role of Ocean Mesoscale Variability in Air-Sea CO2 Exchange: A Global Perspective, Geophysical Research Letters, 51, e2024GL108 373, https://doi.org/10.1029/2024GL108373, 2024.

He, J. and Tyka, M. D.: Limits and CO $_2$ equilibration of near-coast alkalinity enhancement, Biogeosciences, 20, 27–43, https://doi.org/10.5194/bg-20-27-2023, 2023.

Ho, D. T., Bopp, L., Palter, J. B., Long, M. C., Boyd, P. W., Neukermans, G., and Bach, L. T.: Monitoring, reporting, and verification for
690 ocean alkalinity enhancement, State of the Planet, 2-oae2023, 12, https://doi.org/10.5194/sp-2-oae2023-12-2023, 2023.

Humphreys, M. P., Lewis, E. R., Sharp, J. D., and Pierrot, D.: PyCO2SYS v1.8: marine carbonate system calculations in Python, Geoscientific Model Development, 15, 15–43, https://doi.org/10.5194/gmd-15-15-2022, 2022.

Ilyina, T., Wolf-Gladrow, D., Munhoven, G., and Heinze, C.: Assessing the potential of calcium-based artificial ocean alkalinization to mitigate rising atmospheric CO $_2$ and ocean acidification: MODELING MITIGATION POTENTIAL OF AOA, Geophysical Research
695 Letters, 40, 5909–5914, https://doi.org/10.1002/2013GL057981, 2013.

IPCC: Climate Change 2021 – The Physical Science Basis: Working Group I Contribution to the Sixth Assessment Report of the Intergovernmental Panel on Climate Change, Cambridge University Press, 1 edn., ISBN 978-1-009-15789-6, https://doi.org/10.1017/9781009157896, 2021.

IPCC: Climate Change 2022 – Impacts, Adaptation and Vulnerability: Working Group II Contribution to the Sixth Assessment
700 Report of the Intergovernmental Panel on Climate Change, Cambridge University Press, 1 edn., ISBN 978-1-009-32584-4, https://doi.org/10.1017/9781009325844, 2022a.

IPCC, ed.: Climate Change 2022 - Mitigation of Climate Change: Working Group III Contribution to the Sixth Assessment Report of the Intergovernmental Panel on Climate Change, Cambridge University Press, 1 edn., ISBN 978-1-009-15792-6, https://doi.org/10.1017/9781009157926, 2022b.

705 Jeltsch-Thömmes, A., Tran, G., Lienert, S., Keller, D. P., Oschlies, A., and Joos, F.: Earth system responses to carbon dioxide removal as exemplified by ocean alkalinity enhancement: tradeoffs and lags, Environmental Research Letters, 19, 054 054, https://doi.org/10.1088/1748-9326/ad4401, 2024.

Jin, X.-Y. and Cao, L.: Simulated carbon cycle response to ocean iron fertilization and artificial ocean alkalinization, Atmospheric and Oceanic Science Letters, p. 100717, https://doi.org/10.1016/j.aosl.2025.100717, 2025.

710 Keller, D. P., Feng, E. Y., and Oschlies, A.: Potential climate engineering effectiveness and side effects during a high carbon dioxide-emission scenario, Nature Communications, 5, 3304, https://doi.org/10.1038/ncomms4304, 2014.

https://doi.org/10.5194/egusphere-2026-255
Preprint. Discussion started: 22 January 2026

Keller, D. P., Lenton, A., Littleton, E. W., Oschlies, A., Scott, V., and Vaughan, N. E.: The Effects of Carbon Dioxide Removal on the Carbon Cycle, Current Climate Change Reports, 4, 250–265, https://doi.org/10.1007/s40641-018-0104-3, 2018a.

Keller, D. P., Lenton, A., Scott, V., Vaughan, N. E., Bauer, N., Ji, D., Jones, C. D., Kravitz, B., Muri, H., and Zickfeld, K.: The Carbon Dioxide Removal Model Intercomparison Project (CDRMIP): rationale and experimental protocol for CMIP6, Geoscientific Model Development, 11, 1133–1160, https://doi.org/10.5194/gmd-11-1133-2018, 2018b.

Köhler, P.: Anthropogenic CO2 of High Emission Scenario Compensated After 3500 Years of Ocean Alkalinization With an Annually Constant Dissolution of 5 Pg of Olivine, Frontiers in Climate, 2, https://doi.org/10.3389/fclim.2020.575744, 2020.

Köhler, P., Abrams, J. F., Völker, C., Hauck, J., and Wolf-Gladrow, D. A.: Geoengineering impact of open ocean dissolution of olivine on atmospheric CO_2, surface ocean pH and marine biology, Environmental Research Letters, 8, 014 009, https://doi.org/10.1088/1748-9326/8/1/014009, 2013.

Lacroix, F., Burger, F. A., Silvy, Y., Schleussner, C.-F., and Frölicher, T. L.: Persistently Elevated High-Latitude Ocean Temperatures and Global Sea Level Following Temporary Temperature Overshoots, Earth's Future, 12, e2024EF004 862, https://doi.org/10.1029/2024EF004862, 2024.

Lehmann, N. and Bach, L. T.: Global carbonate chemistry gradients reveal a negative feedback on ocean alkalinity enhancement, Nature Geoscience, pp. 1–7, https://doi.org/10.1038/s41561-025-01644-0, 2025.

Lezaun, J.: Hugging the Shore: Tackling Marine Carbon Dioxide Removal as a Local Governance Problem, Frontiers in Climate, 3, 684 063, https://doi.org/10.3389/fclim.2021.684063, 2021.

Martin, K. R., Nickoloff, A., Moffat, L., Weaver, A. J., and Eby, M.: Assessing the effectiveness of ocean alkalinity enhancement on carbon sequestration and ocean acidification, FACETS, 10, 1–8, https://doi.org/10.1139/facets-2024-0171, 2025.

Matthews, H. D., Gillett, N. P., Stott, P. A., and Zickfeld, K.: The proportionality of global warming to cumulative carbon emissions, Nature, 459, 829–832, https://doi.org/10.1038/nature08047, 2009.

Matthews, H. D., Tokarska, K. B., Nicholls, Z. R. J., Rogelj, J., Canadell, J. G., Friedlingstein, P., Frölicher, T. L., Forster, P. M., Gillett, N. P., Ilyina, T., Jackson, R. B., Jones, C. D., Koven, C., Knutti, R., MacDougall, A. H., Meinshausen, M., Mengis, N., Séférian, R., and Zickfeld, K.: Opportunities and challenges in using remaining carbon budgets to guide climate policy, Nature Geoscience, 13, 769–779, https://doi.org/10.1038/s41561-020-00663-3, 2020.

Middelburg, J. J., Soetaert, K., and Hagens, M.: Ocean Alkalinity, Buffering and Biogeochemical Processes, Reviews of Geophysics, 58, e2019RG000 681, https://doi.org/10.1029/2019RG000681, 2020.

Mongin, M., Baird, M. E., Lenton, A., Neill, C., and Akl, J.: Reversing ocean acidification along the Great Barrier Reef using alkalinity injection, Environmental Research Letters, 16, 064 068, https://doi.org/10.1088/1748-9326/ac002d, 2021.

Myhre, G., Highwood, E. J., Shine, K. P., and Stordal, F.: New estimates of radiative forcing due to well mixed greenhouse gases, Geophysical Research Letters, 25, 2715–2718, https://doi.org/10.1029/98GL01908, 1998.

Müller, J. D. and Gruber, N.: Progression of ocean interior acidification over the industrial era, Science Advances, 10, eado3103, https://doi.org/10.1126/sciadv.ado3103, 2024.

Nagwekar, T., Nissen, C., and Hauck, J.: Ocean Alkalinity Enhancement in Deep Water Formation Regions Under Low and High Emission Pathways, Earth's Future, 12, e2023EF004 213, https://doi.org/10.1029/2023EF004213, 2024.

Nagwekar, T., Danek, C., Seifert, M., and Hauck, J.: Alkalinity enhancement in subduction regions and the global ocean: efficiency, earth system feedbacks, and scenario sensitivity, Environmental Research Letters, 21, 014 031, https://doi.org/10.1088/1748-9326/ae293b, 2026.

https://doi.org/10.5194/egusphere-2026-255
Preprint. Discussion started: 22 January 2026

Najjar, R. G. and Orr, J. C.: Design of OCMIP-2 simulations of chlorofluorocarbons , the solubility pump and common biogeochemistry, in: Chemistry, Environmental Science, https://api.semanticscholar.org/CorpusID:39976320, 1998.

National Academies of Sciences, Engineering, and Medicine: A Research Strategy for Ocean-based Carbon Dioxide Removal and Sequestration, National Academies Press, Washington, D.C., ISBN 978-0-309-08761-2, https://doi.org/10.17226/26278, 2022.

Orr, J. C. and Epitalon, J.-M.: Improved routines to model the ocean carbonate system: mocsy 2.0, Geoscientific Model Development, 8, 485–499, https://doi.org/10.5194/gmd-8-485-2015, 2015.

Orr, J. C., Fabry, V. J., Aumont, O., Bopp, L., Doney, S. C., Feely, R. A., Gnanadesikan, A., Gruber, N., Ishida, A., Joos, F., Key, R. M., Lindsay, K., Maier-Reimer, E., Matear, R., Monfray, P., Mouchet, A., Najjar, R. G., Plattner, G.-K., Rodgers, K. B., Sabine, C. L., Sarmiento, J. L., Schlitzer, R., Slater, R. D., Totterdell, I. J., Weirig, M.-F., Yamanaka, Y., and Yool, A.: Anthropogenic ocean acidification over the twenty-first century and its impact on calcifying organisms, Nature, 437, 681–686, https://doi.org/10.1038/nature04095, 2005.

Palmiéri, J. and Yool, A.: Global-Scale Evaluation of Coastal Ocean Alkalinity Enhancement in a Fully Coupled Earth System Model, Earth's Future, 12, e2023EF004 018, https://doi.org/10.1029/2023EF004018, 2024.

Planchat, A., Kwiatkowski, L., Bopp, L., Torres, O., Christian, J. R., Butenschön, M., Lovato, T., Séférian, R., Chamberlain, M. A., Aumont, O., Watanabe, M., Yamamoto, A., Yool, A., Ilyina, T., Tsujino, H., Krumhardt, K. M., Schwinger, J., Tjiputra, J., Dunne, J. P., and Stock, C.: The representation of alkalinity and the carbonate pump from CMIP5 to CMIP6 Earth system models and implications for the carbon cycle, Biogeosciences, 20, 1195–1257, https://doi.org/10.5194/bg-20-1195-2023, 2023.

Qu, B., Song, J., Li, X., Yuan, H., and Duan, L.: Future Changes in Carbon Chemistry Under the Implementation of Artificial Ocean Alkalinization Based on CMIP6 Simulations, Oceans, 6, 29, https://doi.org/10.3390/oceans6020029, 2025.

Renforth, P. and Henderson, G.: Assessing ocean alkalinity for carbon sequestration, Reviews of Geophysics, 55, 636–674, https://doi.org/10.1002/2016RG000533, 2017.

Revelle, R. and Suess, H. E.: Carbon Dioxide Exchange Between Atmosphere and Ocean and the Question of an Increase of Atmospheric CO2 during the Past Decades, Tellus, 9, 18–27, https://doi.org/10.1111/j.2153-3490.1957.tb01849.x, 1957.

Rogelj, J., Forster, P. M., Kriegler, E., Smith, C. J., and Séférian, R.: Estimating and tracking the remaining carbon budget for stringent climate targets, Nature, 571, 335–342, https://doi.org/10.1038/s41586-019-1368-z, 2019.

Sarmiento, J. L. and Gruber, N.: Ocean Biogeochemical Dynamics, Princeton University Press, ISBN 978-0-691-01707-5, https://doi.org/10.2307/j.ctt3fgxqx, 2006.

Sathyanadh, A., Esfandiari, H., Bourgeois, T., Schwinger, J., Bergman, T., Partanen, A.-I., Debolskiy, M., Seifert, M., Keller, D., and Muri, H.: Efficacy of individual and combined terrestrial and marine carbon dioxide removal, Environmental Research Letters, https://iopscience.iop.org/article/10.1088/1748-9326/ae2af5/meta, 2025.

Schwinger, J., Bourgeois, T., and Rickels, W.: On the emission-path dependency of the efficiency of ocean alkalinity enhancement, Environmental Research Letters, 19, 074 067, https://doi.org/10.1088/1748-9326/ad5a27, 2024.

Shevliakova, E., Pacala, S. W., Malyshev, S., Hurtt, G. C., Milly, P. C. D., Caspersen, J. P., Sentman, L. T., Fisk, J. P., Wirth, C., and Crevoisier, C.: Carbon cycling under 300 years of land use change: Importance of the secondary vegetation sink, Global Biogeochemical Cycles, 23, 2007GB003 176, https://doi.org/10.1029/2007GB003176, 2009.

Silvy, Y., Frölicher, T. L., Terhaar, J., Joos, F., Burger, F. A., Lacroix, F., Allen, M., Bernardello, R., Bopp, L., Brovkin, V., Buzan, J. R., Cadule, P., Dix, M., Dunne, J., Friedlingstein, P., Georgievski, G., Hajima, T., Jenkins, S., Kawamiya, M., Kiang, N. Y., Lapin, V., Lee, D., Lerner, P., Mengis, N., Monteiro, E. A., Paynter, D., Peters, G. P., Romanou, A., Schwinger, J., Sparrow, S., Stofferahn, E., Tjiputra,

https://doi.org/10.5194/egusphere-2026-255
Preprint. Discussion started: 22 January 2026

J., Tourigny, E., and Ziehn, T.: AERA-MIP: emission pathways, remaining budgets, and carbon cycle dynamics compatible with 1.5 and 2°C global warming stabilization, Earth System Dynamics, 15, 1591–1628, https://doi.org/10.5194/esd-15-1591-2024, 2024.

Séférian, R., Berthet, S., Yool, A., Palmiéri, J., Bopp, L., Tagliabue, A., Kwiatkowski, L., Aumont, O., Christian, J., Dunne, J., Gehlen, M., Ilyina, T., John, J. G., Li, H., Long, M. C., Luo, J. Y., Nakano, H., Romanou, A., Schwinger, J., Stock, C., Santana-Falcón, Y., Takano, Y., Tjiputra, J., Tsujino, H., Watanabe, M., Wu, T., Wu, F., and Yamamoto, A.: Tracking Improvement in Simulated Marine Biogeochemistry Between CMIP5 and CMIP6, Current Climate Change Reports, 6, 95–119, https://doi.org/10.1007/s40641-020-00160-0, 2020.

Terhaar, J., Frölicher, T. L., Aschwanden, M. T., Friedlingstein, P., and Joos, F.: Adaptive emission reduction approach to reach any global warming target, Nature Climate Change, 12, 1136–1142, https://doi.org/10.1038/s41558-022-01537-9, 2022.

Tyka, M. D.: Efficiency metrics for ocean alkalinity enhancements under responsive and prescribed atmospheric pCO_2 conditions, Biogeosciences, 22, 341–353, https://doi.org/10.5194/bg-22-341-2025, 2025.

Tyka, M. D., Arsdale, C. V., and Platt, J. C.: CO2 capture by pumping surface acidity to the deep ocean, Energy & Environmental Science, 15, 786–798, https://doi.org/10.1039/D1EE01532J, 2022.

van de Mortel, H., Bednaršek, N., Pelletier, G., Feely, R. A., Müller, J. D., and Gruber, N.: Substantial Limitations of Ocean Alkalinity Enhancement in Mitigating the Negative Impacts of Ocean Acidification on Marine Calcifiers, Environmental Science & Technology, https://doi.org/10.1021/acs.est.5c09298, 2025.

Wang, H., Pilcher, D. J., Kearney, K. A., Cross, J. N., Shugart, O. M., Eisaman, M. D., and Carter, B. R.: Simulated Impact of Ocean Alkalinity Enhancement on Atmospheric CO_2 Removal in the Bering Sea, Earth's Future, 11, e2022EF002 816, https://doi.org/10.1029/2022EF002816, 2023.

Wey, H.-W., Moustakis, Y., Nützel, T., Oschlies, A., Schwinger, J., Hajima, T., Fisher, R. A., Ziehn, T., Liddicoat, S. K., Kemena, T. P., and Keller, D. P.: CMIP6 models agree on similar carbon cycle feedbacks between enhancing terrestrial and marine carbon sinks, Environmental Research Letters, 20, 054 029, https://doi.org/10.1088/1748-9326/adc617, 2025.

Winton, M.: A Reformulated Three-Layer Sea Ice Model, Journal of Atmospheric and Oceanic Technology, 17, 525–531, https://doi.org/10.1175/1520-0426(2000)017<0525:ARTLSI>2.0.CO;2, 2000.

Zhou, M., Tyka, M. D., Ho, D. T., Yankovsky, E., Bachman, S., Nicholas, T., Karspeck, A. R., and Long, M. C.: Mapping the global variation in the efficiency of ocean alkalinity enhancement for carbon dioxide removal, Nature Climate Change, pp. 1–7, https://doi.org/10.1038/s41558-024-02179-9, 2024.

Zickfeld, K., Azevedo, D., Mathesius, S., and Matthews, H. D.: Asymmetry in the climate–carbon cycle response to positive and negative CO2 emissions, Nature Climate Change, 11, 613–617, https://doi.org/10.1038/s41558-021-01061-2, 2021.